Title	Chemistry of CO2 Adsorption and Reaction on the Copper Surfaces
Author(s)	Muttaqien, Fahdzi
Citation	大阪大学, 2017, 博士論文
Version Type	VoR
URL	https://doi.org/10.18910/67137
rights	
Note	

Doctoral Dissertation

Chemistry of CO_2 Adsorption and Reaction on the Copper Surfaces

銅表面上における二酸化炭素の吸着と化学反応過程の研究

Fahdzi Muttaqien

July, 2017

Department of Precision Science and Technology
Graduate School of Engineering
Osaka University

ABSTRACT

Many fundamental and practical aspects of CO_2 chemistry on metal surfaces attract considerable attentions due to its important in the industry, energy, and environmental management. Experimental as well as theoretical studies have been conducted to investigate this issue. However, many important aspects are still under debate, *e.g.*, dissociative adsorption of CO_2 and its hydrogenation. As my contribution in these issues, I studied the dissociative adsorption of CO_2 and formate decomposition in my thesis. The thesis is organized as follows: First, I investigated the dissociative adsorption of CO_2 on Cu surfaces. This study is motivated by the experimental evidences of CO_2 dissociation at below 150 K on stepped Cu surface. My thorough analysis showed that CO_2 does not dissociate on "ideal" flat, stepped, and/or kinked Cu surfaces at below 150 K. The CO_2 dissociation on Cu surfaces may be attributed to other factors such as Cu adatoms, gas phase or condensed CO_2, or other gas phase molecules. Particularly, on the stepped and/or kinked Cu surfaces, the CO_2 dissociation may be followed by the $Cu-O-Cu$ chain formation. Next, I investigated the CO_2 adsorption on the Cu surfaces from density functional theory calculations as well as the temperature programmed desorption and X-ray photoelectron spectroscopy studies. Several exchange-correlation functionals have been considered to characterize CO_2 adsorption on the copper surfaces. I used the van der Waals density functionals (vdW-DFs), *i.e.*, the original vdW-DF (vdW-DF1), optB86b-vdW, and rev-vdW-DF2, as well as the PBE with dispersion correction (PBE-D2). It is found that vdW-DF1 and rev-vdW-DF2 functionals slightly underestimate the equilibrium adsorption energy, while PBE-D2 and optB86b-vdW functionals give better agreement with the experimental estimation for CO_2 on Cu(111). The calculated CO_2 adsorption energies on the flat, stepped, and kinked Cu surfaces are in the range $20 - 27$ kJ/mol, which are compatible with the general notion of physisorbed species on solid surfaces. Last but not least, I performed *ab initio* molecular dynamics analysis of formate decomposition to CO_2 and H on the Cu(111) surface to elucidate the enhancement factors of formate synthesis. Here, I showed that the desorbed CO_2 has approximately twice larger bending vibrational energy than the translational, rotational, and stretching vibrational energies. Since formate synthesis, the reverse reaction of formate decomposition, had been suggested experimentally to occur by the Eley-Rideal mechanism, I propose that the formate synthesis can be enhanced if the bending vibrational mode of CO_2 is excited rather than the translational and/or stretching vibrational modes. Detailed information on CO_2 adsorption and energy distribution of desorbed CO_2 may inspire new insights into improving catalytic activity of synthesis of formate.

This page is intentionally left blank.

I dedicate this work to my beloved wife and parents.

This page is intentionally left blank.

CONTENTS

LIST OF TABLES

LIST OF FIGURES

This page is intentionally left blank.

Chapter 1

Introduction

1.1 CO_2 chemistry on Cu based catalyst

In the industrial technical processes, carbon dioxide is used in the limited four chemical reactions: producing the fertilizer from CO_2 interaction with ammonia, pharmaceutical and pesticides production via the Kolbe-Schmitt process from CO_2 and sodium phenolate, production of polyacryl fibres, and methanol synthesis from CO_2 hydrogenation.[1] The limitation of CO_2 usage is due to its rather low energy content compared with carbon monoxide. The impetus for investigating the prospects of carbon dioxide may also come from the basic demand of energy. The fast depletion of fossil fuel urges us to explore new energy sources. From the last decade, the solar energy, biomass, geothermal source, and nuclear power plant have been chosen to replace the fossil fuel. In addition to those renewable energy resources, methanol has been also considered as a promising one.[2–5]

In industry, methanol and/or higher alcohols are produced through CO_2 or CO hyrogenation on metal catalysts.[2,6,7] Copper based catalyst is a typical catalyst that is used to support the catalytic reaction of methanol synthesis. In fact, methanol synthesis consists of several elementary reaction steps. However, CO_2 adsorption must be the first elementary step in the reaction sequence of methanol synthesis. Therefore, understanding the CO_2 adsorption chemistry on catalyst surfaces becomes fundamentally important as the initial stage in evaluating further complex reactions.

One of the most important elementary reactions in the methanol sythesis is CO_2 hydrogenation into formate (HCOO).[8–12] The interesting issue of fomate synthesis is the fact that this reaction is consistent with an Eley-Rideal (ER) type mechanism.[13–16] The ER mechanism suggests that formate synthesis can be enhanced by controlling the initial impinging energy of CO_2. One possible way to elucidate the appropriate initial impinging energy of CO_2 is by investigating the dynamics of CO_2 itself from formate decomposition, which is reverse reaction of formate synthesis. Therefore, elucidation of formate decomposition dynamics is important for improving catalytic formate synthesis.

As my contribution in the CO_2 chemistry field, I studied two important issues related with CO_2 that may disclose the fundamental aspect beyond them. First, I studied the dissociative adsorption of CO_2 on the Cu surfaces. Second, I studied the dynamics of CO_2 desorption as a product formate decomposition on Cu(111). The elucidation of CO_2 dynamics as formate decomposition product is important to enlighten us about the key factors that can improve formate synthesis and/or methanol synthesis in general.

1.2 Thesis structure

My thesis is contructed based on the published and in peer review works.

- **Chapter 2** focuses on the dissociative adsorption on the flat, stepped, and kinked Cu surfaces. Several possible reaction paths of CO_2 dissociation are presented in this chapter. Proposed reaction schematic of Cu−O−Cu chain formation is also presented in this chapter.

- **Chapter 3** focuses on CO_2 adsorption on the Cu surfaces from density functional theory calculations as well as the temperature programmed desorption and X-ray photoelectron spectroscopy.

- **Chapter 4** focuses on the dynamics of desorbed CO_2 as a product formate decomposition. The energy transfer into CO_2 translation, vibration, and rotation modes is discussed in here.

- **Chapter 5** summarizes all the results and proposes some future plan.

Chapter 2

Dissociative Adsorption of CO_2 on Flat, Stepped, and Kinked Cu Surface

2.1 Background

Adsorption and reaction of CO_2 on solid surfaces are attracting growing interest because of their importance in industrial, energy, and environmental problems.[5,17] In industry, H_2, CO_2 and CO gas mixtures are used in methanol synthesis by using $Cu/ZnO/Al_2O_3$ catalysts,[18,19] where CO_2 is considered to be the main carbon source on the basis of the results of an isotope labeling experiment.[18] Another well known reaction that involves CO_2 is the reverse water gas shift reactions (RWGS) reaction.[20] The RWGS is an endothermic reaction that includes chemical interaction between CO_2 and catalyst surface. Therefore, study of CO_2 adsorption and dissociation (Fig. 2.1) on solid surfaces is important in industry applications.

A number of studies on CO_2 adsorption on single crystal copper surfaces have been done previously. On the flat copper surface, CO_2 is weakly adsorbed and needs high activation energy to dissociate. It was reported that the CO_2 activation energy is 0.69 eV on the Cu(110) at 400-600 K[21] and 0.96 eV on the Cu(100) at 500 K.[22] Even at 45 K and subsequent heating up to 120 K, CO and oxygen species were not found on the Cu(110) within the detection limit of HREELS and AES.[23] On the other hand, from temperature programmed desorption (TPD) spectra, Fu and Somorjai reported that CO_2 is adsorbed and dissociated to CO and O on the Cu(311) surface at 4 L dose and 150 K.[24] Bönicke *et al.* also showed that CO_2 is chemisorbed and dissociates at 95 K over the Cu(332) surface by means of thermal desorption spectroscopy (TDS) experiment.[25] Koitaya and co-workers reported that CO_2 is dissociated on the Cu(997) surface at 83 K by infrared reflection absorption spectroscopy (IRAS).[26] They exposed isotopically-labelled $^{13}CO_2$ to the Cu(997) surface at 83 K and observed two absorption peaks at 2050 cm^{-1} and 2066 cm^{-1}, which are assigned to C$-$O stretching mode of ^{13}CO at terrace and step sites, respectively. This phenomenon clearly demonstrate the dissociation of CO_2 at low temperature. They also reported no CO_2 dissociation on the Cu(111) surface at this temperature.

There have been a few theoretical studies related with CO_2 dissociative adsorption. Cao *et al.* reported some reaction paths of CO_2 dissociation on the Ni(211) surface.[27] Also, the unfavorable CO_2 dissociative adsorption over $Cu_2O(111)$ was reported previously.[28] Meanwhile, its reverse reaction, CO oxidation, had been studied for the flat, stepped, and kinked metal surfaces comprehensively.[29–31] However, the detail of CO_2 dissociation reactions over clean copper surfaces have not been reported and remain obscure. Especially, it is not clear whether the CO_2 dissociation takes place at stepped copper surfaces at low temperature. This process is fundamentally important as basic science because CO_2 is a typical molecule and copper surface is a typical component of the catalyst commonly used in industry. Furthermore, the defects on surface are considered to be active sites for catalytic reactions.[19,32,33]

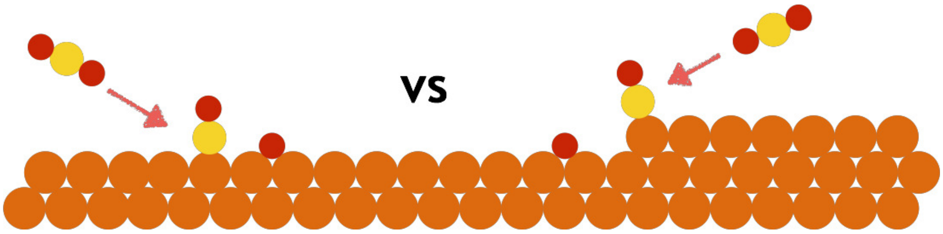

Figure 2.1: CO_2 dissociation on the terrace region and near the step edge of metal surface.

2.2 Objectives

In this chapter, I discuss CO_2 dissociative adsorption on the flat, stepped, and kinked copper surfaces by means of density functional theory (DFT). Additionally, I also considered the roles of metal adatom and pre-adsorbed oxygen atom in the dissociation process. By investigating such complexity, we can understand the catalytic activity of copper surface in the "real" condition at low temperature in the experiment laboratory.

2.3 Computational details

The minimum energy pathways (MEP) of CO_2 dissociation has been considered on the flat Cu(111), stepped Cu(221) and Cu(211), and kinked Cu(11 5 9) surfaces. The flat, stepped, and kinked Cu surfaces were constructed using $3 \times 2\sqrt{3}$, 3×1, 3×1, and 1×1 unit cells, respectively. We sampled the surface Brillouin zone by using a uniform grid of $(4 \times 4 \times 1)$, $(4 \times 4 \times 1)$, $(4 \times 3 \times 1)$, and $(6 \times 4 \times 1)$ k-points, respectively. The three close-packed layers (with a fixed bottom atomic layer) was used for the slab models. The distance between two neighboring slabs in the surface normal direction is 30 Å, which is sufficient to prevent undesired interaction. The slab surfaces were constructed by using a calculated equilibrium lattice constant of 3.65 Å, which is close to the experimental value of 3.62 Å.[34]

The MEP of the CO_2 dissociation process were obtained using the nudged elastic band (NEB) method.[35] The climbing image NEB (CI-NEB) method[36] was performed only for the highest saddle point. At the beginning, I constructed $10-12$ images between the initial and final states. After $120-140$ molecular dynamic iterations, one new image was added if the distance between two adjacent old images is more than 1 Å. The standard GGA Perdew-Burke-Ernzerhof (GGA-PBE)[37] exchange-correlation functional was used. The electron-ion interaction was described using Vanderbilt's ultrasoft pseudopotentials.[38] The energy cutoffs of the plane wave basis sets are 25 Ry and 225 Ry for wave function and charge density, respectively. The dispersion correction proposed by Grimme (DFT-D2)[39] was used to describe the dispersion interaction between Cu surface and CO_2 molecule. All calculations were carried out by using the STATE (Simulation Tool for Atom TEchnology) package, which previously has been applied to the synthesis of formate and its hydrogenation process.[32,33,40]

The vibrational frequencies of the adsorbed species were calculated using frozen phonon approximation. For higher accuracy, the energy cutoffs of the plane wave basis sets were incresed up to 36 Ry and 400 Ry for wave function and charge density, respectively. The metal surface was fixed in the relaxed geometry, and the 0.026 Å adsorbate displacement was taken as the initial step size of the finite difference as the basis for the Hessian matrix. Then, the corresponding vibrational normal modes can be obtained by solving Wilson's non-symmetric secular equation.[41]

In particular, CO adsorption on the flat and stepped Cu surfaces was investigated since it becomes the main product of CO_2 dissociation. The van der Waals density functional (vdW-DF)[42,43] was used in the post-processing calculations to avoid the "CO adsorption puzzle".[44] The vdW-DF calculations were applied to charge density data obtained from standard GGA-PBE calculations. The revised Perdew-Burke-Ernzerhof (revPBE)[45] exchange functional was used in the vdW-DF calculations. For higher accuracy, the surface thickness was increased to six close-packed layers. The energy cutoffs of the plane wave basis sets are 36 Ry and 400 Ry for wave function and charge density, respectively.

2.4 Results and discussions

2.4.1 CO adsorption

In this section, the CO adsorption energies obtained from standard GGA-PBE and vdW-DF calculations were compared. The CO adsorption energies are calculated based on the following definition

$$E_{\mathrm{ads}}^{\mathrm{CO}} = E_{\mathrm{tot}}(\mathrm{sys}) - [E_{\mathrm{tot}}(\mathrm{subs}) + E_{\mathrm{tot}}(\mathrm{CO})], \tag{2.1}$$

where $E_{\mathrm{tot}}(\mathrm{sys})$, $E_{\mathrm{tot}}(\mathrm{subs})$, and $E_{\mathrm{tot}}(\mathrm{CO})$ represent the total energies of the adsorbed system, the clean relaxed substrate, and gas phase CO, respectively. Meanwhile, the CO adsorption energies obtained from the vdW-DF calculations followed the reported prescriptions to eliminate error due to the "egg-box effect", *i.e.*, the dependence of the total energies on the positions of atoms relative to the fast Fourier transform (FFT) grid points[46,47]

$$\begin{aligned} E_{\mathrm{ads}}^{\mathrm{CO}} &= E_{\mathrm{tot}}^{\mathrm{vdW}}(\mathrm{sys}) - E_{\mathrm{fix}}^{\mathrm{vdW}}(\mathrm{subs}) - E_{\mathrm{fix}}^{\mathrm{vdW}}(\mathrm{ads}) \\ &\quad + [E_{\mathrm{fix}}^{\mathrm{GGA}}(\mathrm{subs}) - E_{\mathrm{tot}}^{\mathrm{GGA}}(\mathrm{subs})] + [E_{\mathrm{fix}}^{\mathrm{GGA}}(\mathrm{ads}) - E_{\mathrm{tot}}^{\mathrm{GGA}}(\mathrm{ads})], \end{aligned} \tag{2.2}$$

where $E_{\mathrm{tot}}^{\mathrm{vdW}}(\mathrm{sys})$, $E_{\mathrm{tot}}^{\mathrm{GGA}}(\mathrm{subs})$, and $E_{\mathrm{tot}}^{\mathrm{GGA}}(\mathrm{ads})$ represent the total energies of the adsorbed system, the isolated clean substrate, and the gas phase adsorbate, respectively. The $E_{\mathrm{fix}}^{\mathrm{GGA/vdW}}(\mathrm{subs})$ and $E_{\mathrm{fix}}^{\mathrm{GGA/vdW}}(\mathrm{ads})$ represent the total energies of the clean substrate and the gas phase adsorbate with their geometries fixed to those in the optimized adsorbed systems. The superscripts "GGA" and "vdW" mean that the total energies were obtained from DFT calculations with self-consistent GGA-PBE and from post-processing vdW-DF calculations, respectively.

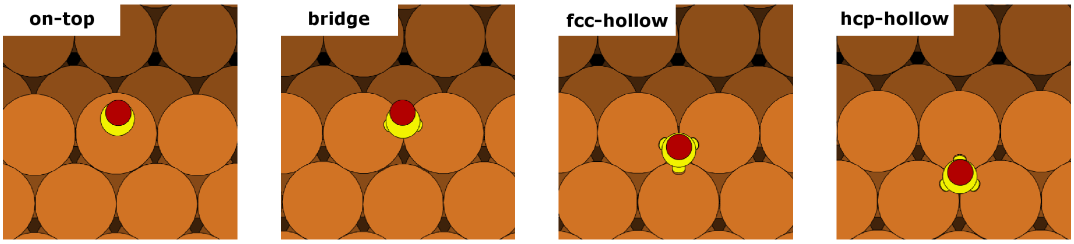

Figure 2.2: CO molecule adsorption sites on the Cu(221) surface. Red, yellow, and brown spheres represent oxygen, carbon, and copper atoms, respectively.

Figure 2.2 shows four possible CO adsorption sites on the Cu(221) surface. The one most favorable for CO adsorption is the on-top site, which agrees with previously reported experimental results.[48–50] As shown in Table 2.1, the vdW-DF produces more accurate predictions of the most stable state of CO on copper surfaces than the standard

Table 2.1: Calculated CO adsorption energies ($E_{\text{ads}}^{\text{CO}}$), CO vibrational frequencies (ν(C−O)) and C−O bond length ($d_{\text{C-O}}$) for stable adsorption sites. The vdW-DF calculation results are shown in square brackets. More negative the adsorption energy means stronger and more attractive interaction with the surface.

Ads. site	$E_{\text{ads}}^{\text{CO}}$ (eV)		ν(C−O) (cm^{-1})		$d_{\text{C-O}}$ (Å)	
	Cu(111)	Cu(221)	Cu(111)	Cu(221)	Cu(111)	Cu(221)
top	−0.73 [−0.46]	−0.92 [−0.62]	2047	2061	1.16	1.16
fcc	−0.78 [−0.41]	−0.86 [−0.45]	1854	1814	1.19	1.19
hcp	−0.72 [−0.41]	−0.89 [−0.41]	1852	1795	1.19	1.19
bridge	−0.68 [−0.38]	−0.88 [−0.54]	1892	1902	1.18	1.18
Exp.	−0.49[49]	−0.59[49]	2078[52,53]	2089[54]	1.13[55]	-

GGA-PBE calculations. The GGA-PBE predicts fcc-hollow site as the most stable CO adsorption site on Cu(111), while vdW-DF predict the on-top site. These results are similar to those of a previous theoretical study.[44] Both GGA-PBE and vdW-DF suggest that an on-top-edge site is the most favorable CO adsorption site on the Cu(221) surface. A previous study using standard GGA found that the most stable CO adsorption site is an on-top site of the step edge.[50,51] The calculated CO adsorption energy for an on-top-edge site of Cu(221) using vdW-DF is 0.16 eV more stable than that of an on-top site of Cu(111). A previous study using thermal desorption spectroscopy found that the CO adsorption energy for the on-top-edge is 0.10 eV more stable than that for the on-top site of terrace region,[49] which is in good agreement with the present calculation results.

The vibrational frequencies of CO molecules (ν(C-O)) on all possible adsorption sites were then calculated. The calculated vibrational frequencies of CO at the on-top site decreases by 80 − 100 cm^{-1} from its gas phase value (2143 cm^{-1})[52] (shown in the Table 2.1), which are in good agreement with previous experimental results. The CO vibrational frequency decreases to 2078 cm^{-1} and 2089 cm^{-1} after it adsorbs on Cu(111)[52,53] and Cu(211)[54] surfaces, respectively. The decrease in the CO stretching mode is due to electron transfer between the surface and adsorbate. The decrease in frequency is also accompanied by elongation of the C−O bond in both the flat and stepped Cu surfaces.

As shown in Table 2.1, the elongation of C−O bonds for the on-top site is quite small compared with the experimental results for an isolated system (1.13 Å).[55] The C−O bond length for the on-top site agrees well with that of a previous theoretical study (1.16 Å).[31] The C−O bond lengths for the bridge and hollow sites are longer than for the on-top site.

2.4.2 CO_2 dissociation on clean flat, stepped, and kinked Cu surfaces

2.4.2.1 CO_2 dissociation on Cu(111)

At the initial, CO_2 is weakly adsorbed on the Cu(111) surface. The calculated relative distance between the surface and CO_2 is more than 3 Å, which is much larger than the copper-carbon distance for the on-top site in the CO adsorption case (1.85 Å). The calculated vibrational frequency of the O−C−O asymmetric stretching mode of CO_2 on the Cu(111) surface (Table 2.2) is in the range of its vibrational frequencies in the gas phase (2349 cm^{-1} - 2396 cm^{-1}).[56,57] These results then strengthens that CO_2 is physisorbed on the Cu(111) surface.

By constructing the transition state (TS) and performing NEB calculations, I investigated the CO_2 dissociation process on the Cu(111) surface. Figure 2.3 shows the schematic structure of the minimum energy path of CO_2 dissociation on the Cu(111) surface. At the final state (FS), the adsorption sites for dissociated CO and oxygen atoms are the on-top site and fcc-hollow site, respectively. The stability of the dissociated products is indicated by the energy difference between the initial and final states (ΔE). As shown in the Table 2.2, the FS is 0.81 eV less stable than the initial state (IS). The calculated CO_2 activation energy (E_a) on the Cu(111) surface is 1.33 eV. A quite large CO_2 activation energy on the Cu(111) surface has been also indirectly reported in the CO oxidation reactions.[29,30] The corresponding MEP of CO_2 dissociation processes on Cu(111) can be seen in Fig. 2.4. This figure also shows the deformation of O−C−O bond angle and C−O bond length, and the distance between closest copper atom to the adsorbed molecule during the dissociation process. Along the increase of reaction coordinate, the CO_2 starts approaching to the surface and becomes less stable. During this process, the CO_2 bends and the C-O bond (noted as C−O1 in Fig. 2.4) slightly elongates. At the saddle point, the bond angle almost reaches 110° and the dissociated products are adsorbed on the metal surface, thus the C−O1 bond length becomes larger. Judging from the calculated activation energy, CO_2 dissociation is not favorable at low temperature on Cu(111).

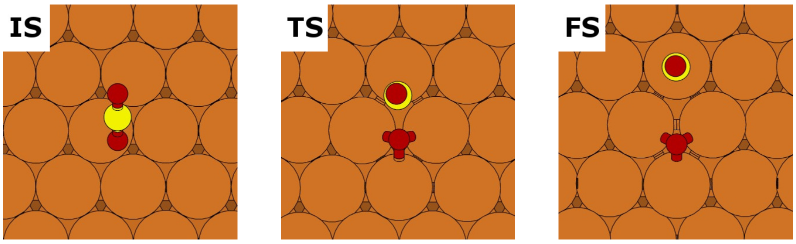

Figure 2.3: Schematic of dissociative adsorption process of CO_2 on the Cu(111) surface. From left to right: initial state (IS), transition state (TS), and final state (FS).

2.4.2.2 CO_2 dissociation on Cu(221)

By creating various transition and final states on the stepped Cu(221) surface, I constructed four possible reaction paths of CO_2 dissociation. These reaction paths are denoted by "Model1", "Model2", "Model3", and "Model4" (shown in the Fig. 2.5). The CO_2 is weakly adsorbed on the stepped surfaces and the dissociated products are less stable than the initial ones even if the dissociated CO species are located at the on-top site of copper atoms. The characteristic of CO_2 adsorption at the IS for all models is identified by its relative distance from the surface, which is more than 3 Å, and its vibrational frequencies, which are similar with its in the isolated gas phase. The stability of the FS of each model and CO_2 vibrational frequencies are listed in Table 2.2.

The calculated CO_2 activation energies on Cu(221) are slightly lower than those on Cu(111). The calculated activation energy of CO_2 dissociation on Model1 and Model2 is 1.06 eV. A similar activation energy was also reported indirectly in the CO oxidation on Cu(311).[31] The activation energies for Model3 and Model4 are 1.57 eV and 1.72 eV, respectively (Table 2.2). The considered MEP of all reaction paths on Cu(221) are similar with those on Cu(111). Figure 2.6 shows one of example of MEP for reaction path of Model2. As shown in this figure, the total energy increases simultaneously while the CO_2 approaches to the surface and starts bending. The C−O bond (noted as C-O1 in Fig. 2.6) also elongates during bending process. At the transition states, the CO_2 bond angle reaches below 120° and the C−O bond length becomes longer. Judging from the calculated activation energies, the CO_2 dissociation is also not favorable at low temperature even on stepped surface.

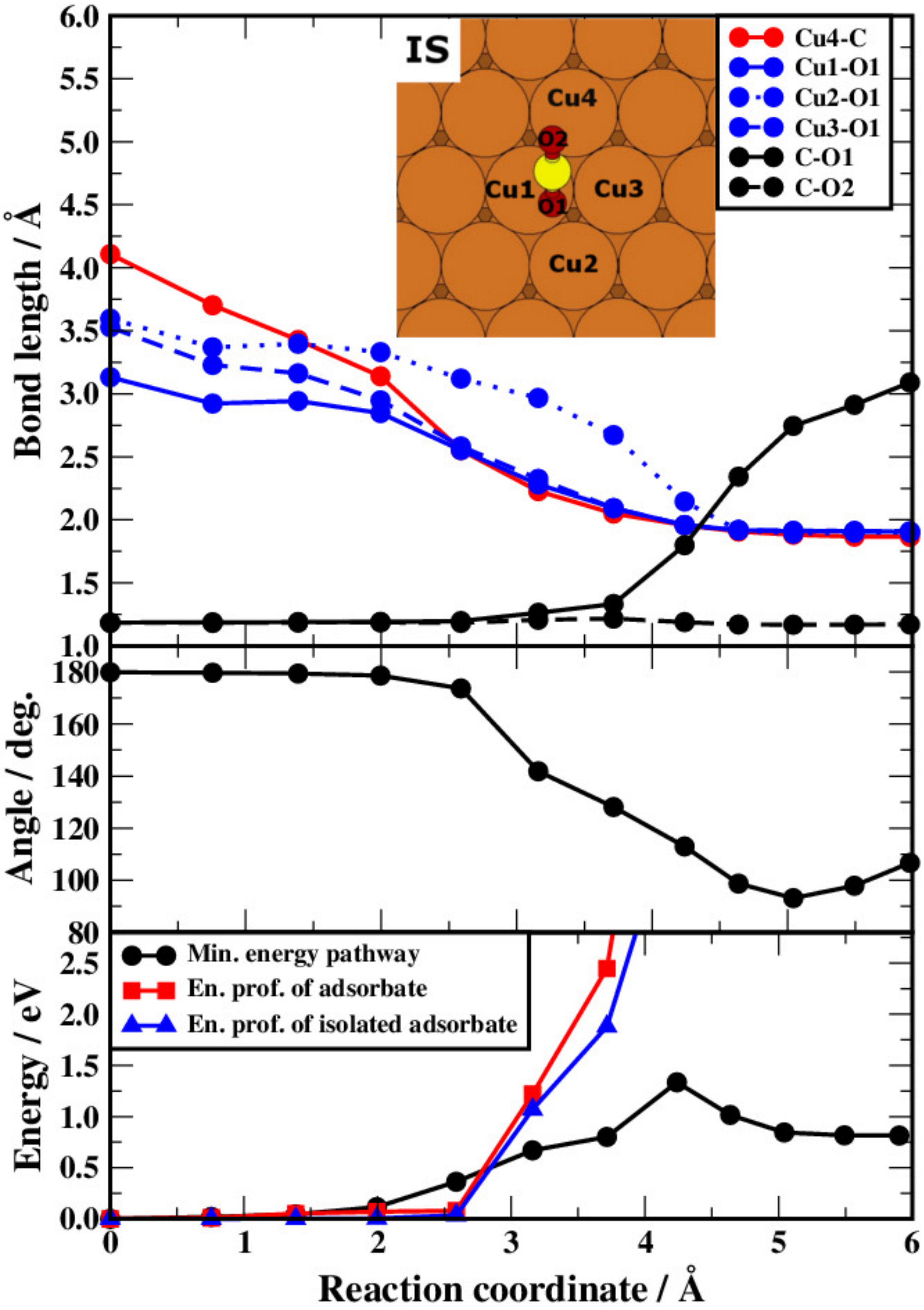

Figure 2.4: From bottom to top panels: minimum energy pathway and energy profile of adsorbate and isolated adsorbate, O−C−O bond angle profile, and C−O bond length profile of the CO_2 dissociation processes on the Cu(111) surface, respectively. The reaction coordinate in horizontal axis is defined as the distance of each replica from the initial state along the minimum energy path obtained from NEB calculations. Inset: representative atomic numbering for measuring the bond distances.

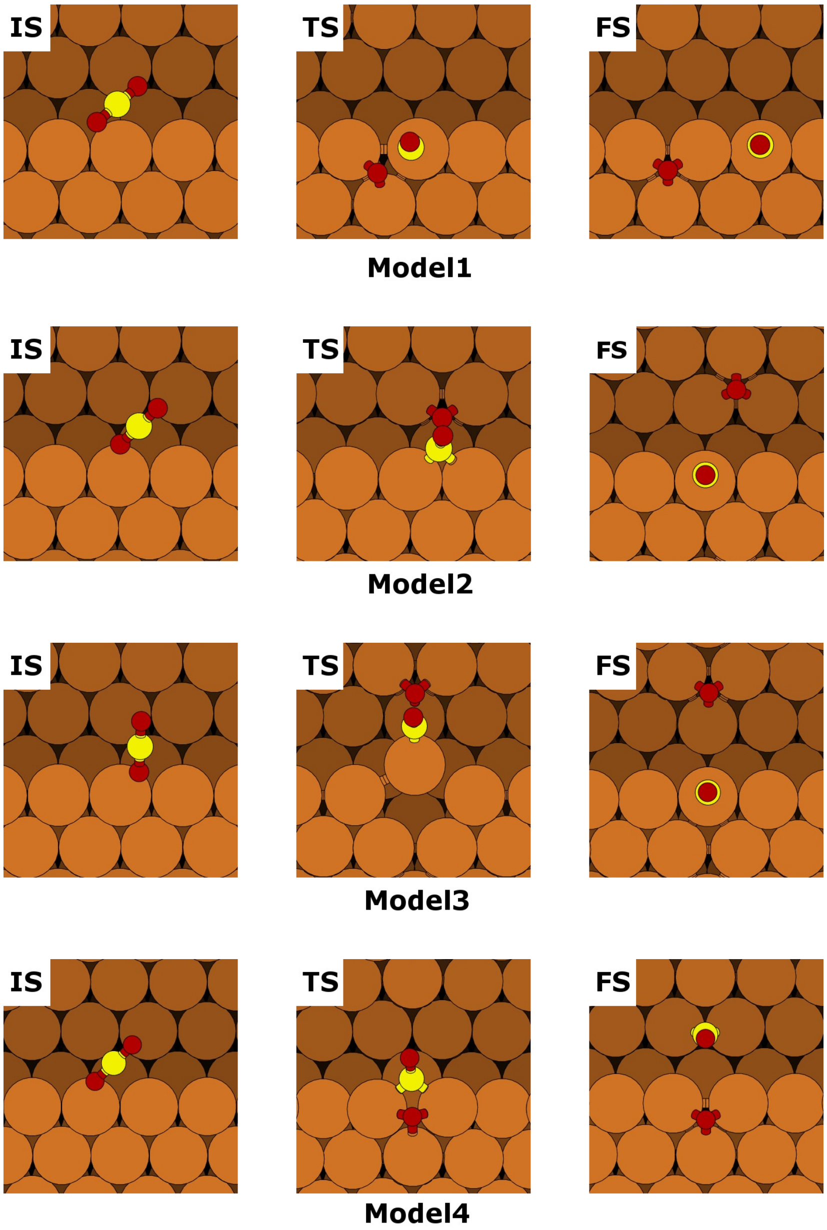

Figure 2.5: Schematic of dissociative adsorption process of CO_2 on the Cu(221) surface. From left to right: initial state (IS), transition state (TS), and final state (FS).

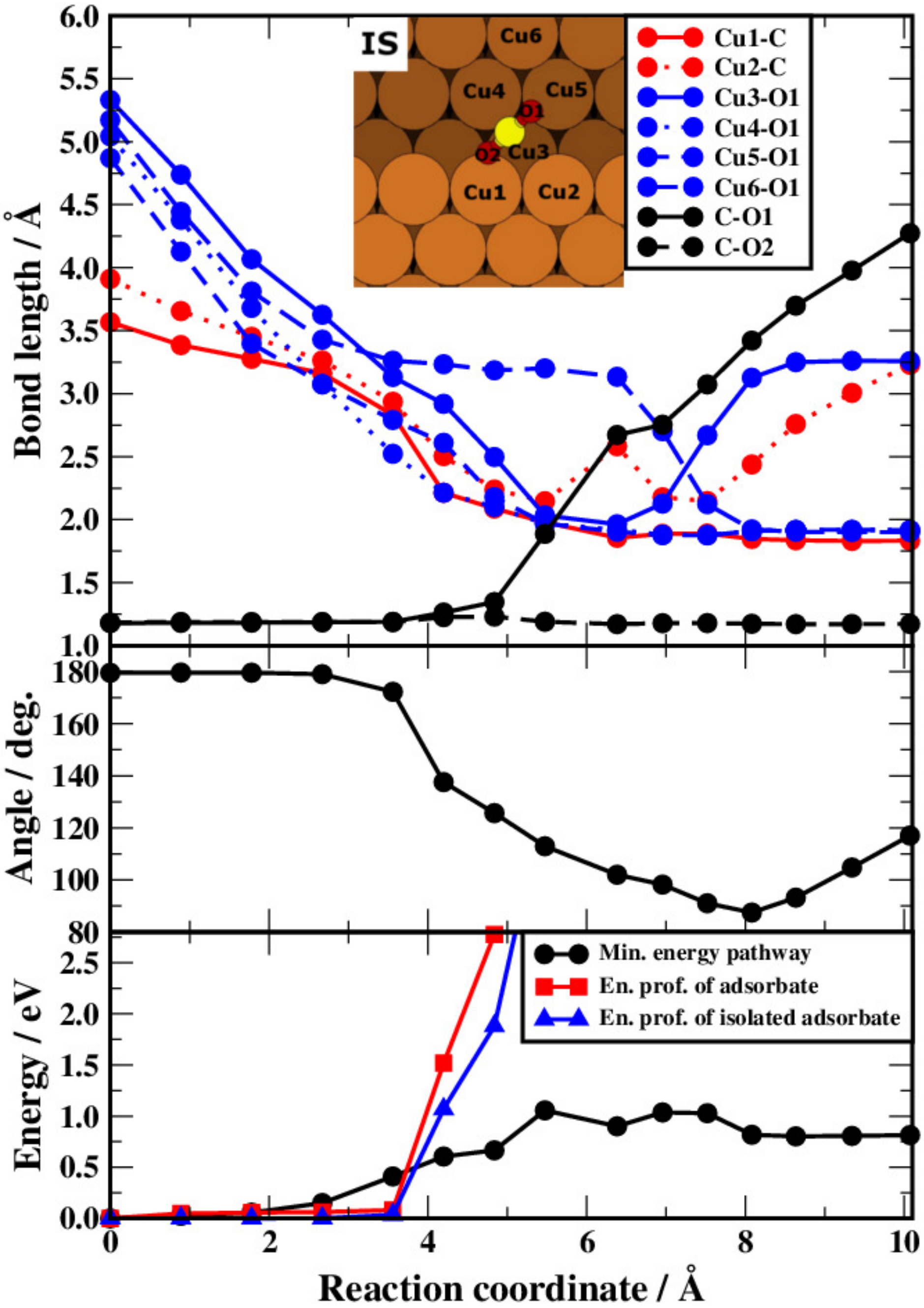

Figure 2.6: From bottom to top panels: minimum energy pathway and energy profile of adsorbate and isolated adsorbate, O-C-O bond angle profile, and C-O bond length profile of Model2 for CO_2 dissociation on the Cu(221) surface, respectively. Inset: representative atomic numbering for measuring the bond distances.

2.4.2.3 CO_2 dissociation on Cu(211)

The CO_2 dissociative adsorption on Cu(211) is discussed in this section. The Cu(211) surface has a (100) facet structure at the step edge (Fig. 2.7). On the basis of the results on Cu(221), I considered two reaction paths by including the step edge atoms in the TS. At the IS, CO_2 is also weakly adsorbed on Cu(211) and its O−C−O asymmetric stretching modes (Table 2.2) are similar with its isolated gas phase molecule. The relative distance between CO_2 and surface at the IS of these two models is more than 3 Å, which again indicates that CO_2 is weakly adsorbed on the surface.

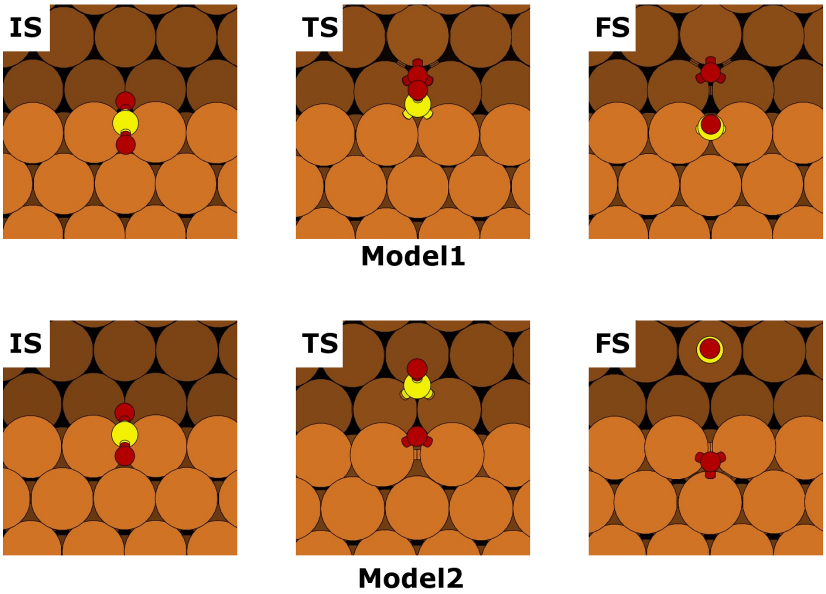

Figure 2.7: Schematic of dissociative adsorption process of CO_2 on the Cu(211) surface. From left to right: initial state (IS), transition state (TS), and final state (FS).

The proposed reaction paths for the Cu(211) surface are shown in Fig. 2.7. They are denoted by “Model1” and “Model2”. Unlike the previous stepped surface, the CO_2 activation energy decreases substantially on the Cu(211) surface. The calculated activation energies are 0.67 eV and 1.35 eV for Model1 and Model2, respectively. The Model1 has a 0.66 eV lower activation energy compare with CO_2 dissociation on Cu(111). As CO_2 is weakly adsorbed in the IS, the MEP profiles in Fig. 2.8 also shows similar criterion with the dissociation processes on the Cu(111) and Cu(221) surfaces. The barrier energy increases quite significant when CO_2 bond angle turns to 140°.

The post-processing of vdW calculations were then performed on the Model1 of Cu(211) since it has the lowest activation energy. The vdW-DF calculations were done to obtain higher accuracy in determining the activation energy of CO_2 dissociation. The calculated activation energy for this model is 1.11 eV. The total energy difference between the IS and FS for this model is increased by using the vdW-DF functional. Once again, present post-processing calculations indicate that CO_2 dissociation is not

Table 2.2: Calculated vibrational frequencies of asymmetric O−C−O stretching mode of CO_2 (ν(O−C−O)) in the initial state, C-O stretching mode of CO (ν(C−O)) in the final state, energy difference between the final and the initial products (ΔE), CO and the oxygen atom adsorption energy in the transition state ($E_{\mathrm{ads}}^{\mathrm{TS}}$(CO) and $E_{\mathrm{ads}}^{\mathrm{TS}}$(O)), interaction energy in the transition state ($E_{\mathrm{int}}^{\mathrm{TS}}$), the activation energy (E_{a}) of CO_2 dissociation, and CO oxidation (reverse reactions) energy ($E_{\mathrm{oxi}}^{\mathrm{CO}}$) of possible reaction paths. The vdW-DF calculation results are shown in square brackets.

	ν(O−C−O) (cm^{-1})	ν(C−O) (cm^{-1})	ΔE (eV)	$E_{\mathrm{ads}}^{\mathrm{TS}}$(CO) (eV)	$E_{\mathrm{ads}}^{\mathrm{TS}}$(O) (eV)	$E_{\mathrm{int}}^{\mathrm{TS}}$ (eV)	E_{a} (eV)	$E_{\mathrm{oxi}}^{\mathrm{CO}}$ (eV)
				Cu(111)				
	2391	2077	0.81	−0.54	−2.01	−0.20	1.33	0.52
				Cu(221)				
Model1	2386	2075	0.36	−0.97	−2.20	0.13	1.06	0.70
Model2	2395	2056	0.81	−0.88	−2.00	−0.22	1.06	0.24
Model3	2395	2084	0.57	0.21	−1.38	−1.35	1.57	1.00
Model4	2396	1866	0.70	−0.77	−2.06	0.40	1.72	1.02
				Cu(211)				
Model1	2384	1953	0.60 [1.04]	−1.02	−2.19	−0.23	0.67 [1.11]	0.07 [0.06]
Model2	2384	2059	0.70	−0.58	−1.98	−0.20	1.35	0.66
				Cu(11 5 9)				
Model1	2235	2052	0.88	−0.87	−2.02	−0.11	1.21	0.33
Model2	2235	1920	0.96	−0.96	−1.98	−0.24	1.03	0.08
Model3	2235	2098	0.89	−0.74	−2.04	−0.40	1.02	0.14

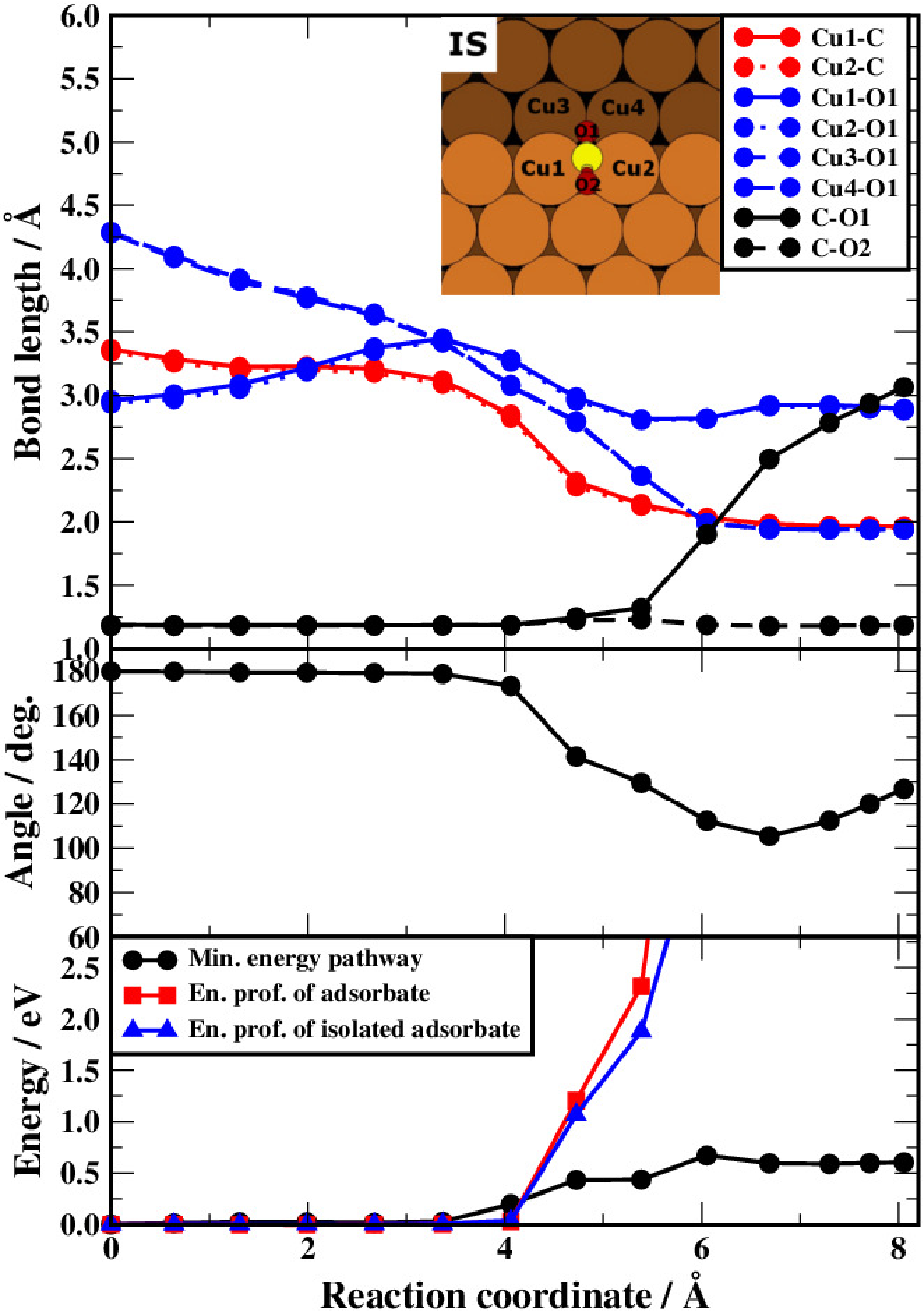

Figure 2.8: From bottom to top panels: minimum energy pathway and energy profile of adsorbate and isolated adsorbate, O−C−O bond angle profile, and C−O bond length profile of Model1 for CO_2 dissociation on the Cu(211) surface, respectively. Inset: representative atomic numbering for measuring the bond distances.

likely on the Cu(211) surface at low temperature.

2.4.2.4 CO_2 dissociation on Cu(11 5 9)

In this section, I discuss the CO_2 dissociative adsorption on the kinked Cu(11 5 9) surface. I investigated three possible dissociation paths as shown in Fig. 2.9. They are denoted as “Model1”, “Model2”, and “Model3”. The CO_2 is weakly adsorbed on the kinked surface at the IS. The relative distance between the metal surface and the CO_2 in the initial state is more than 3 Å. The calculated CO_2 stretching modes (Table 2.2) for the Cu(11 5 9) surface are 150 cm^{-1} lower than that of the flat and stepped surfaces.

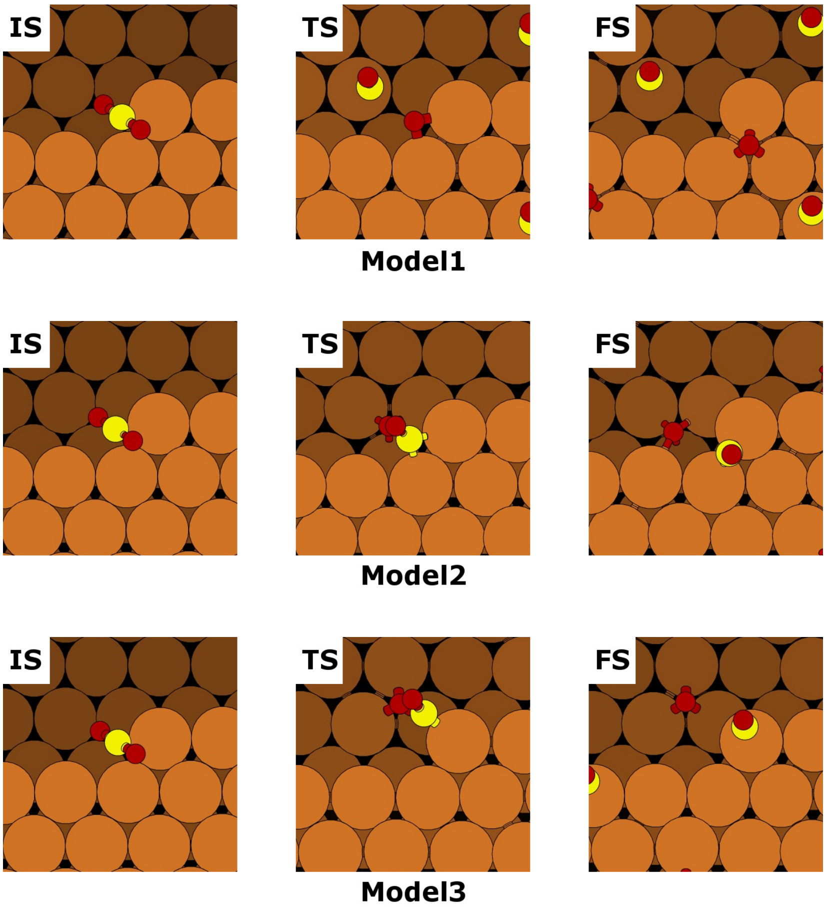

Figure 2.9: Schematic of dissociative adsorption process of CO_2 on the Cu(11 5 9) surface. From left to right: initial state (IS), transition state (TS), and final state (FS).

The calculated activation energies are 1.21 eV, 1.03 eV and 1.02 eV for Model1, Model2, and Model3, respectively (Table 2.2). The calculated activation energies for Model2 and Model3 are similar to that for Model2 of Cu(221). As can be seen in the MEP profiles of Model3 (Fig. 2.10), the system becomes less stable when the CO_2 molecule starts approaching to the surface and its O−C−O structure starts bending.

Again, the total energy increases when the adsorbate bends and C−O bond length also elongates.

The calculated barrier energies increase quite significantly when the CO_2 bond angle becomes 140°. Actually, this behavior is happened to all considered reaction paths. Therefore, I tried to confirm the consequence of CO_2 bending to the barrier energy. I removed the metal surface and fixed the CO_2 geometry as its stable configuration based on NEB calculations (shown as red-square line in the lower panel of Figs. 2.4, 2.6, 2.8, and 2.10). Also, I calculated the isolated CO_2 system with various bond angle and fixed the C-O bond length as its stable bond length configuration in the gas phase of 1.16 Å (shown as blue-triangle line in the lower panel of Figs. 2.4, 2.6, 2.8, and 2.10). The isolated adsorbate system becomes unstable when its bond angle turns to less than 140°. It discloses that CO_2 bond angle deformation gives significant contribution in the increasing of CO_2 dissociation activation energy. The step and kink sites are not enough to reduce the barrier height due to CO_2 bond angle deformation. Unfortunately, the bending of CO_2 is inevitable since the CO_2 needs to bend while it approaches to the surface.

Several reaction paths have been optimized to elucidate the CO_2 dissociation on the flat, stepped, and kinked copper surfaces. The calculated barrier energies of CO_2 dissociation are 1.33 eV, 1.06 eV, 0.67 eV, and 1.02 eV on Cu(111), Cu(221), Cu(211), and Cu(11 5 9) surfaces, respectively. The present GGA-PBE functional is known to underestimate the activation barriers slightly, thus the vdW-DF calculations are necessary to check the accuracy of the calculations. The barrier height on the Cu(211) surface is increased from 0.67 eV to 1.11 eV by including vdW corrections. Our calculated results are in reasonable agreement with experimentally reported activation energies for low-index Cu surfaces, *i.e.*, 0.69 eV for Cu(110)[21] and 0.96 eV for Cu(100)[22]. Although I thoroughly investigated the dissociation process for CO_2 on flat, stepped, and kinked copper surfaces, the barrier height never dropped below 0.60 eV. I thus conclude that CO_2 does not dissociate on ideally flat, ideally stepped or ideally kinked copper surfaces. The origin of the discrepancy between our theoretical results and experimental observations for the dissociative adsorption of CO_2 on stepped surfaces is not clear at present. In the present theoretical simulations, I used "ideally" flat, stepped, and kinked surfaces. In contrast, on "real" surfaces, more complex processes such as step fluctuation, adatom diffusion, and adsorbate enhanced metal diffusion might be involved.[58,59] Therefore, I also investigated the roles of adatoms on the surfaces in the CO_2 dissociation processes.

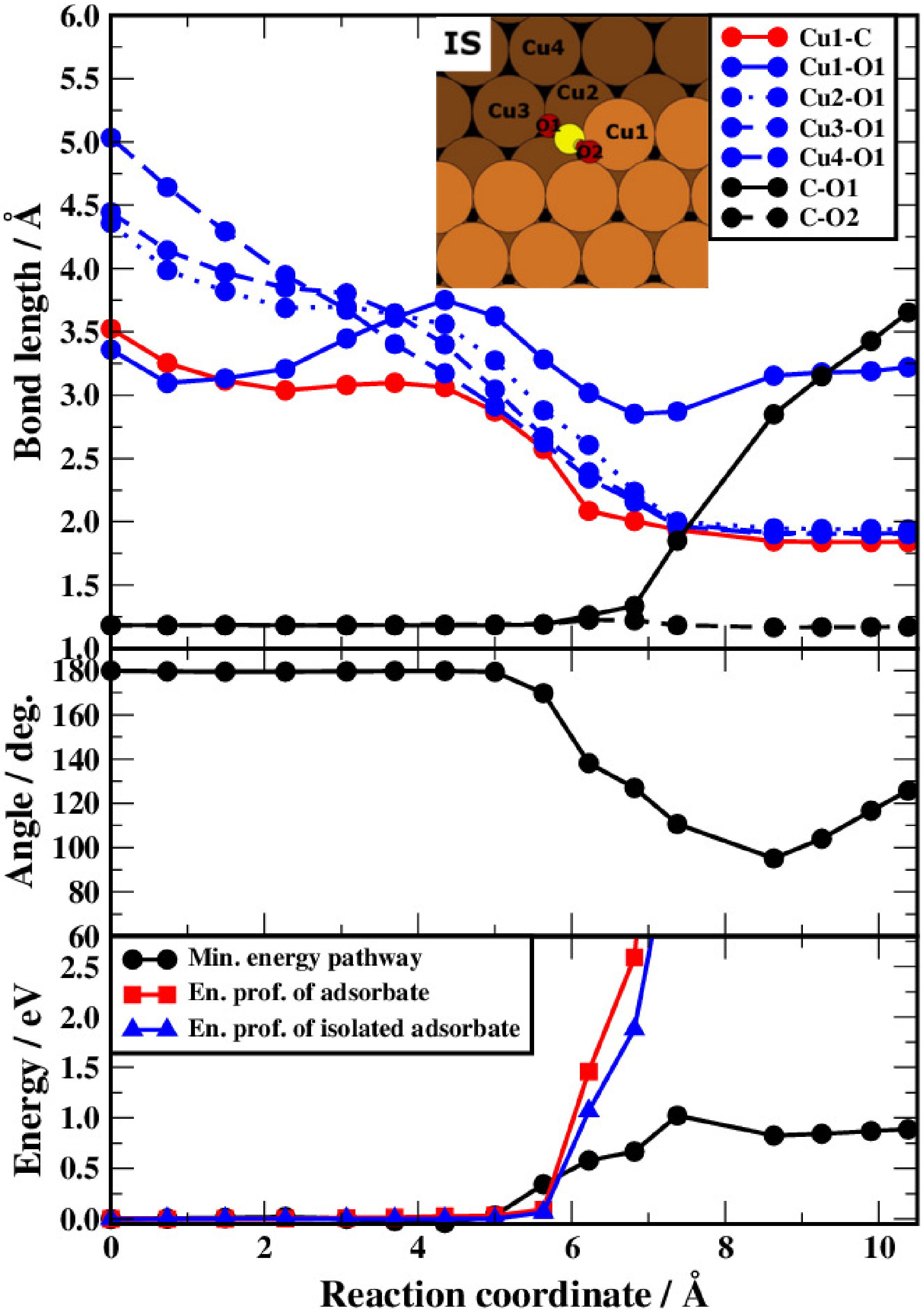

Figure 2.10: From bottom to top panels: minimum energy pathway and energy profile of adsorbate and isolated adsorbate, O−C−O bond angle profile, and C−O bond length profile of Model3 for CO_2 dissociation on the Cu(11 5 9) surface, respectively. Inset: representative atomic numbering for measuring the bond distances.

2.4.3 CO_2 dissociation on surfaces with adatoms

2.4.3.1 Roles of Cu adatoms in the CO_2 dissociation on Cu(221) surface

In order to figure out the discrepancy between the theoretical results and experimental observations, I considered more complex models as experimental conditions by considering adatoms on the surfaces. On “real” surfaces, more complex processes such as step fluctuation, adatom diffusion, and adsorbate enhanced metal diffusion might be involved.[58,59] Thus, I added one and two adatoms on the Cu(221) surface, and optimized the IS and FS for CO_2 dissociation. At the initial, CO_2 is physisorbed on the surface. Meanwhile, I propose that the dissociated oxygen atom forms small Cu−O−Cu chain at the FS.

Two reaction paths regarding the CO_2 dissociation on the copper surface with adatoms have been optimized. The proposed reaction paths can be seen in Fig. 2.11. In the case of one Cu adatom, the final state is 0.49 eV less stable than the initial state. Figure 2.12a shows the MEP and bond angle profile of CO_2 dissociation processes on copper surface with one adatom. The intermediate state (IM) was obtained in the first reaction path. I observed downhill energy path in the beginning of processes and then it gradually increases when the CO_2 bond angle is close to 140°. However, the transition state is slightly more stable than the initial state even the CO_2 bond angle is deformed to nearly 140°. The energy profile continuously increases along with CO_2 bond angle deformation until it dissociates. The effective activation energy from the intermediate state to the highest peak (TS2) is 1.04 eV (Table 2.3), which is 0.29 eV lower than the activation energy on clean Cu(111) surface and slightly lower than on the clean Cu(221) surface. Based on these results, it is concluded that Cu adatoms can suppress the barrier height due to bond angle deformation. However, the calculated activation energy for this reaction path suggests that the CO_2 is still not favorable to dissociate at low temperature.

The CO_2 activation energy for the second reaction path with two Cu adatoms is 0.62 eV (Table 2.3). At the IS of this reaction path, two Cu adatoms are located on the fcc hollow site (as shown in Fig. 2.11) and the CO_2 is in its gas phase state. The dissociated oxygen atom and two Cu adatoms form small Cu−O−Cu chain at the final state. Figure 2.12b shows the MEP and bond angle profile for this reaction path. At the beginning, there is downhill energy pathway, and then the barrier increases about 0.18 eV. The increase in barrier energy is because one copper adatom shifts to another stable state, which is on hcp hollow site (see TS1 of two adatoms case in Fig. 2.11). After pass this TS1, the barrier height fluctuates and the CO_2 bond angle drop below 140°. Interestingly, there is no high barrier even the CO_2 bond angle deforms much further until it is nearly 120°. Right after that, the barrier is dramatically increased until the system reaches TS2 point. This behavior contradicts with CO_2 case

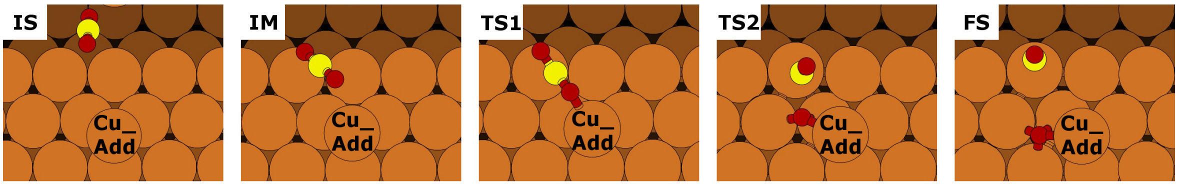

One Copper Adatom

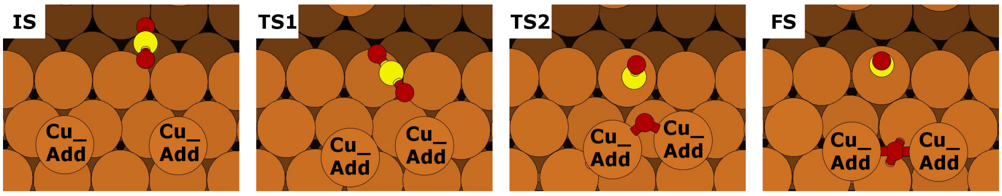

Two Copper Adatoms

Figure 2.11: Schematic of dissociative adsorption process of CO_2 on Cu(221) surface with one and two copper adatoms. The "IM" label in the figure means intermediate state.

on clean Cu surfaces, where the barrier increases when the CO_2 bond angle turns to 140°. The copper adatoms play important roles to retain the system stability when CO_2 approaches to the surface and its bond angle deformed. Though, the calculated activation energy for this reaction path suggests that the CO_2 is also still not favorable to dissociate at low temperature.

We also proposed another reaction path related with copper adatoms on the surface as shown in Fig. 2.13. At the IS, I constructed small Cu−O−Cu chain and one copper adatom on the surface, and CO_2 is in its gas phase state. Based on the MEP in Fig. 2.14, we can see small peak when CO_2 bonds with copper adatom in TS1. The presence of small peak is because of the distortion of copper adatom from its stable position and due to CO_2 bond angle deformation. The IM was observed in this reaction path, which is more stable than the IS even though the CO_2 bond angle deformation is nearly 120°. Interestingly, the effective activation energy (from IM to the TS2 points) of this reaction path is 0.48 eV, which is 0.85 eV and 0.19 eV lower that that of clean Cu(111) and Cu(211) surfaces case, respectively. Thus, the copper adatoms are effective treatment to retain the system stability against CO_2 bond angle deformation.

2.4.3.2 Behind Cu−O−Cu chain formation: CO_2 dissociation

The Cu−O−Cu chain formation was considered as a possible model of CO_2 dissociation process on copper surfaces with adatoms. The idea of Cu−O−Cu chain formation was initiated from our results in the previous subsection that copper adatoms can reduce the barrier height due to CO_2 bond angle deformation. Therefore, in the last section, we investigated the CO_2 dissociation in the Cu−O−Cu chain formation processes.

In this model, I have two CO_2 and one of them is already adsorbed on the surface.

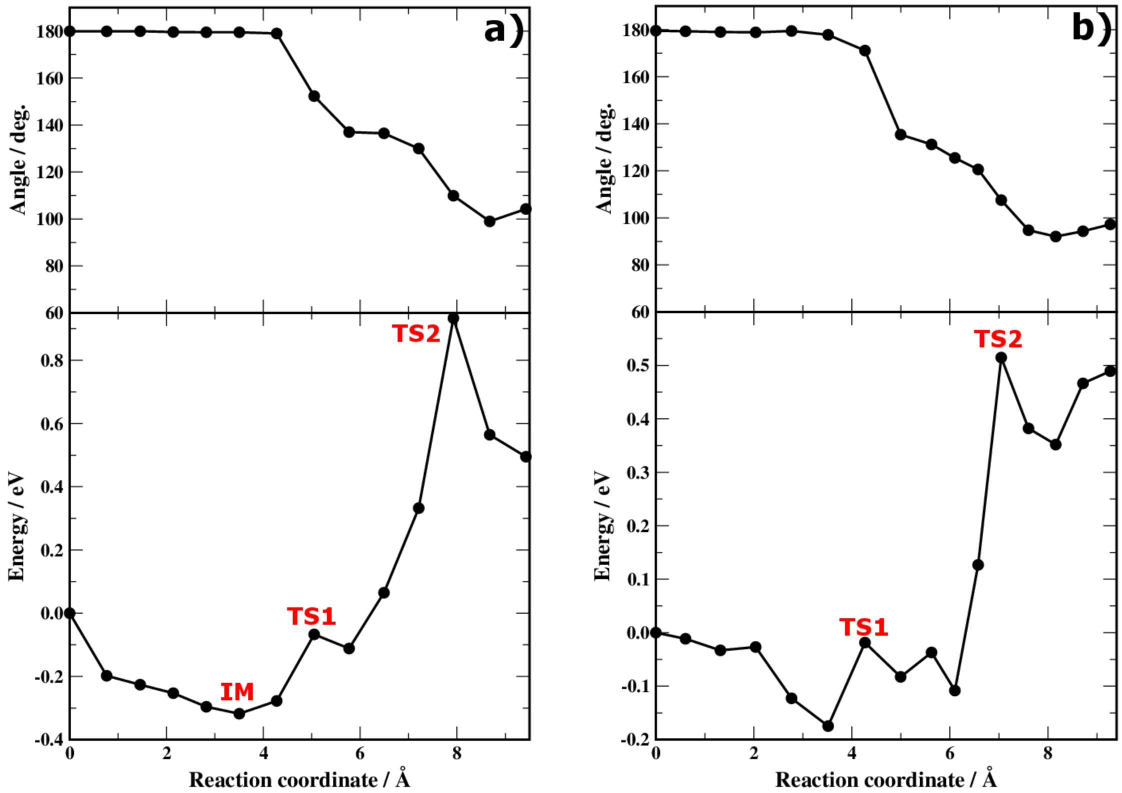

Figure 2.12: From bottom to top panels: minimum energy pathway and O−C−O bond angle profile for CO_2 dissociation, respectively, on the Cu(221) surface with (a) one copper adatom and (b) two copper adatoms.

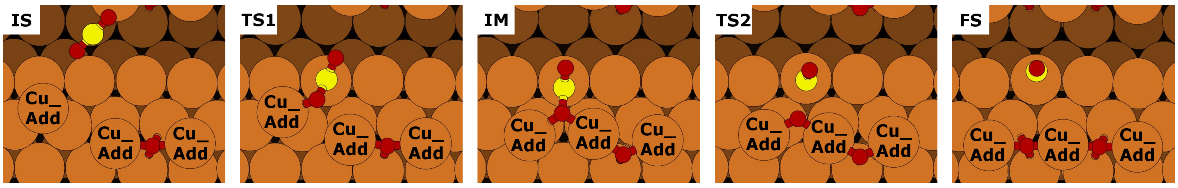

Figure 2.13: Schematic of dissociative adsorption process of CO_2 on Cu(221) surface with one copper adatom and small CuO chain.

Table 2.3: Calculated vibrational frequencies of asymmetric O-C-O stretching mode of CO_2 (ν(O−C−O)) in the initial state, energy difference between the final and the initial states (ΔE), and the activation energy (E_a) of CO_2 dissociation process.

	ν(O−C−O) (cm^{-1})	ΔE (eV)	E_a (eV)
One Cu adatom	2406	0.49	1.04
Two Cu adatoms	2395	0.49	0.62
Adatom + small Cu−O chain	2403	0.07	0.48
Long Cu−O chain	1649	0.23	0.46

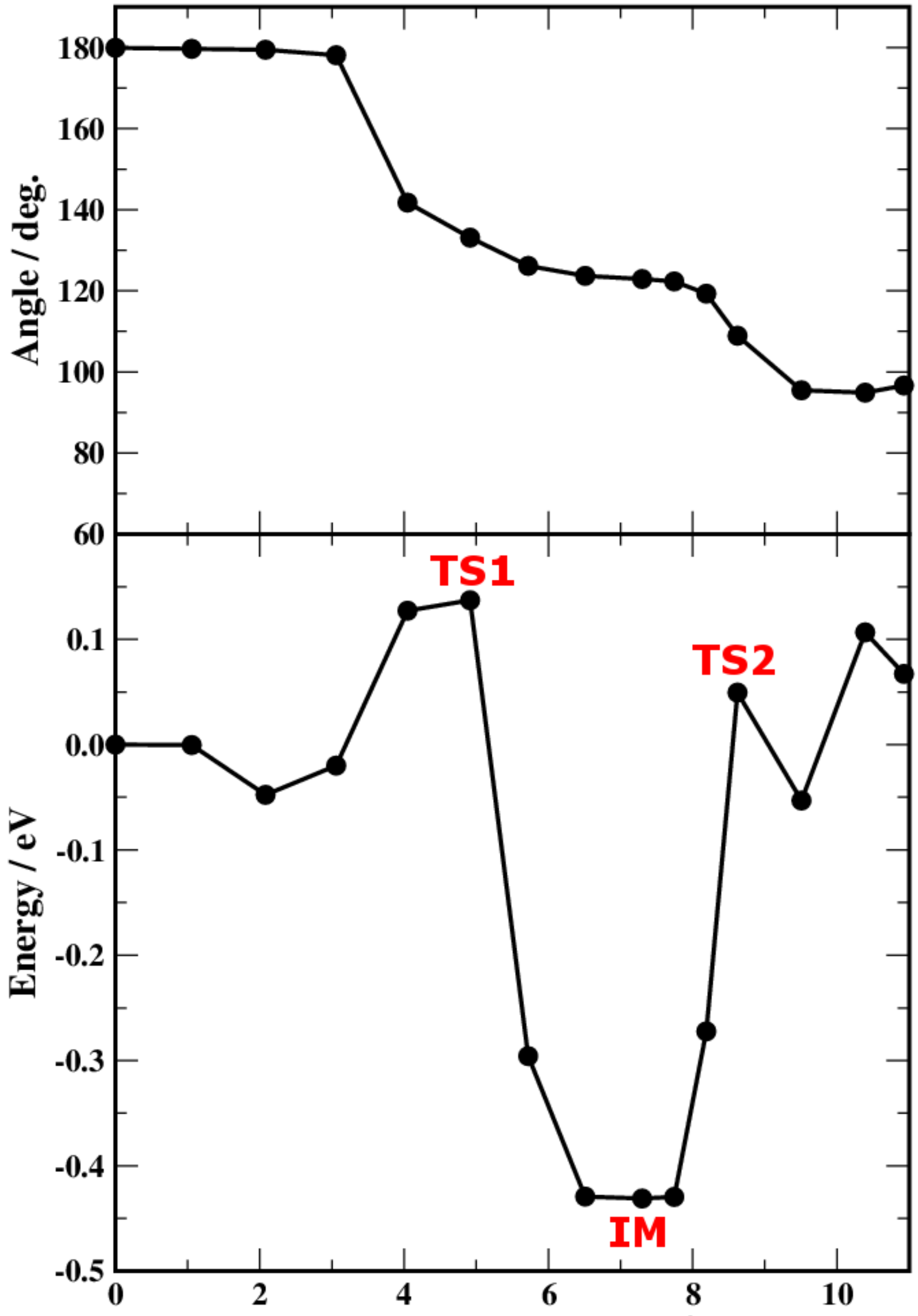

Figure 2.14: From bottom to top panels: minimum energy pathway and O-C-O bond angle profile for CO_2 dissociation on the Cu(221) surface with one copper adatom and small CuO chain, respectively.

In addition, there are small Cu−O−Cu chain and one copper adatom as the initial state. Meanwhile, at the final state, one CO_2 dissociated and another adsorbed at the end of Cu−O−Cu chain on the surface as shown in the schematic in Fig. 2.15. Figure 2.16 shows the energy pathway of this reaction model. Again, an intermediate state was observed in this reaction path. There is 0.25 eV barrier before the system reaches the intermediate state. At the IM, two CO_2 molecules adsorb on the surface and their bond angle is quite similar. The precursor of Cu−O−Cu chain is formed in this reaction path and then one CO_2 is dissociated. The calculated activation energy from intermediate state to the highest peak is 0.28 eV. However, the activation energy of this reaction path is 0.46 eV (Table 2.3), which is 1.27 and 0.21 eV lower than that of clean Cu(111) and Cu(211) surfaces case, respectively.

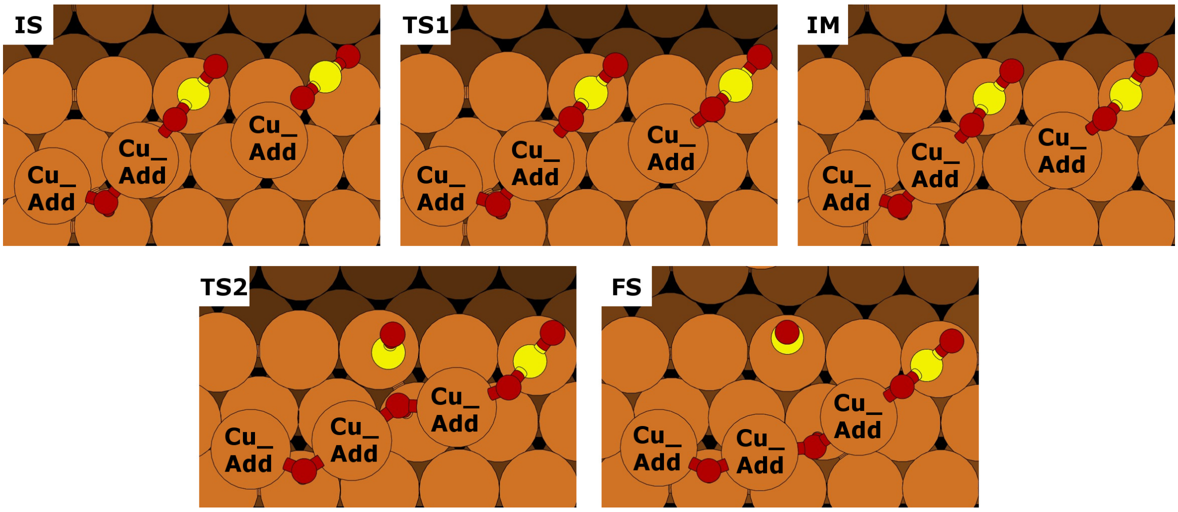

Figure 2.15: Schematic of dissociative adsorption process of CO_2 during Cu−O−Cu chain formation on Cu(221) surface.

The surface defects such as steps or kinks are not enough to reduce the activation energy of CO_2 dissociation at low temperature based on present theoretical study. There is one important factor which causes why the activation energies are never below 0.67 eV on the ideally clean flat, stepped, or kinked copper surfaces. Since the CO_2 is weakly adsorbed on the ideally clean copper surfaces, the barrier height always increases when CO_2 approaches to the surface and makes bond with it. The effect of deformation of CO_2 bond angle will not reduce unless the copper adatoms are introduced on the surface.

2.5 Summaries

I have investigated the dissociation process of CO_2 to CO + O on the Cu(111), Cu(221), Cu(211), and Cu(11 5 9) surfaces by using DFT-GGA and vdW-DF calculations. The

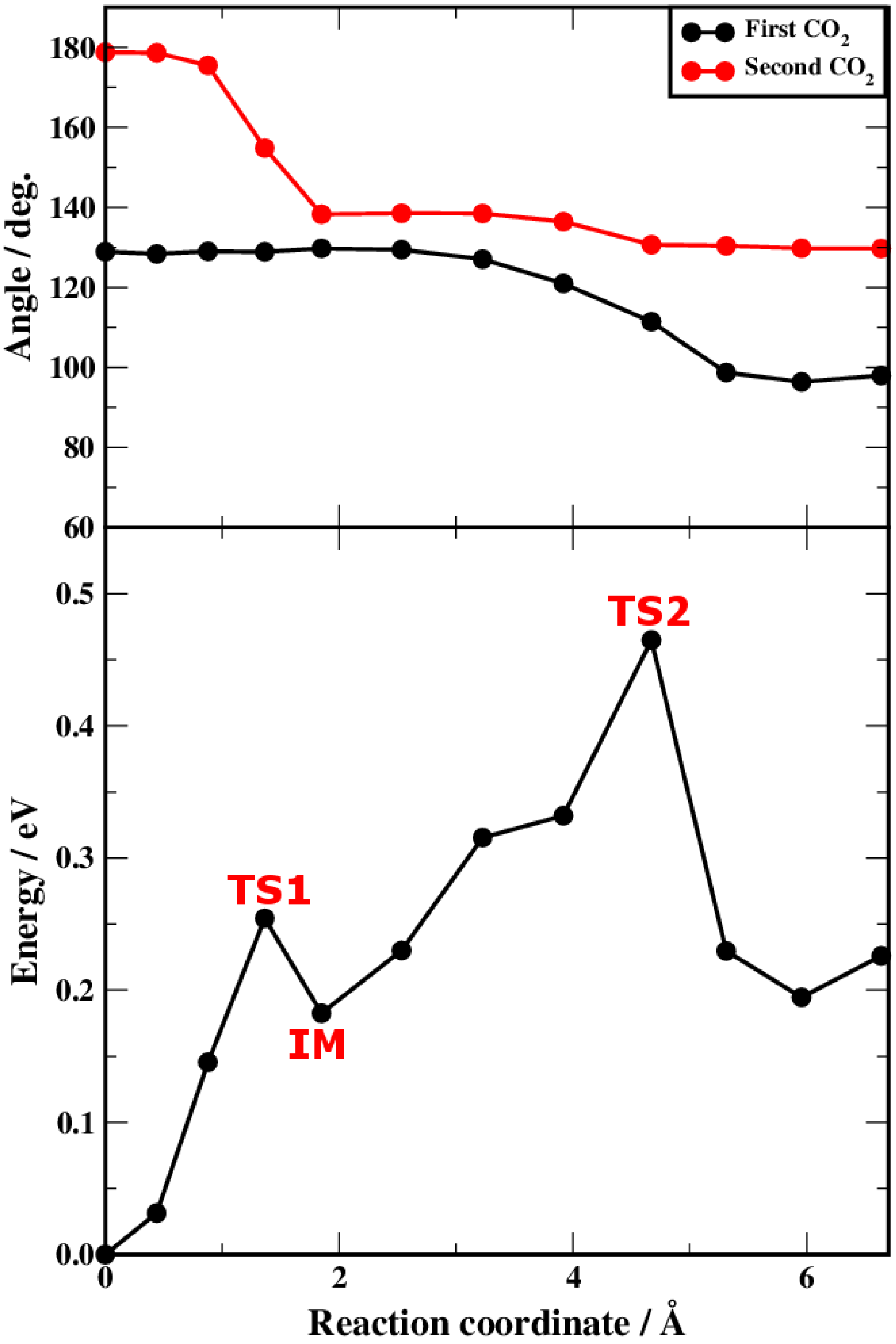

Figure 2.16: From bottom to top panels: minimum energy pathway and O−C−O bond angle profile for CO_2 dissociation during CuO chain formation on Cu(221) surface, respectively. The first CO_2 refers to the one that dissociates, meanwhile the second CO_2 refers to the otherwise.

activation energy for CO_2 dissociation on the flat Cu(111) surface is 1.33 eV, which agrees well with previous reports. For stepped and kinked surfaces, the activation energies are slightly lower, 1.06 eV, 0.67 eV, and 1.02 eV for the Cu(221), Cu(211), and Cu(11 5 9) surfaces, respectively. Based on the present calculations, CO_2 does not dissociate on the "ideally" flat, stepped or kinked Cu surfaces at low temperature. The deformation of CO_2 bond angle gives significant effect to the height of activation energies.

The adatoms on the surface give remarkable effect on the CO_2 activation energy. The adatoms are able to reduce the barrier height of the dissociation adsorption of CO_2. The CO_2 activation energies on Cu(221) surface with one and two copper adatoms are 1.04 eV and 0.62 eV, respectively. In the other case, when small Cu−O−Cu chain already formed on the surface, the next CO_2 activation energy is reduced to 0.48 eV. Therefore, I suggest that the CO_2 dissociation may be followed by the Cu−O−Cu chain formation. These may be the first attempt to introduce the effect of Cu−O−Cu chain in the CO_2 dissociation on Cu surfaces.

This page is intentionally left blank.

Chapter 3

van der Waals Density Functional and TPD Studies of CO_2 Adsorption on the Copper Surfaces

3.1 Background

The chemistry of CO_2 on solid surfaces has received great attention due to its importance in a variety of applications in catalysis, energy, and environmental management.[2,5] One of leading CO_2 management is the conversion of this greenhouse gas into more valuable compound. In industry, CO_2 is hydrogenated into methanol and/or higher alcohols on metal catalysts.[2,6–10] Moreover, CO_2 is also a main reactant in reverse water gas shift (RWGS) reaction, methane synthesis, and methane reforming reaction to produce hydrogen for amonia synthesis. In such complex reactions, the first elementary step in the reaction processes is the adsorption of CO_2. Thus, understanding CO_2 adsorption on catalysts surfaces becomes fundamentally important in evaluating further complex reactions.

In the past few years, many thorough studies have been performed to investigate CO_2 adsorption on catalysts surfaces. The typical model relevant to many industrial scale chemical reactions is CO_2 adsorption on Cu surfaces.[21,23,24,60–66] On low-index Cu surfaces, *i.e.*, Cu(100) and Cu(110), CO_2 is physisorbed at rather low temperature with measured adsorption energies of 26−30 kJ/mol[65] and 21 kJ/mol,[23] respectively. On the other hand, the stepped Cu surfaces have higher activity for CO_2 adsorption. CO_2 is dissociatively adsorbed on the stepped Cu(311) at 150 K and on Cu(332) at 95 K under UHV condition.[24,64] Interestingly at temperature below 70 K, vibrational modes of CO_2 physisorbed on stepped Cu(997) show asymmetric Fano-line shapes, which indicates electronic coupling between Cu surface and vibrational modes of CO_2.[60]

The theoretical investigation of CO_2 adsorption on the Cu surfaces is quite limited. The adsorption energy of CO_2 on low-index Cu surfaces follows this common trend:

Cu(110) > Cu(100) > Cu(111),[67] according to the previous density functional theory (DFT) studies with local density approximation (LDA) and generalized gradient approximation (GGA) based functionals. Despite standard GGA functionals are widely used to elucidate complex chemical reaction such as CO_2 hydrogenation,[10,11,68,69] these functionals inaccurately describe weakly bound systems, *i.e.*, benzene and naphthalene on graphite,[70] benzene on noble metal surfaces,[71] and pentacene on Cu(111).[72] Additionally, GGA functionals are also unable to predict correct CO adsorption site on precious metal surfaces (CO adsorption puzzle).[73] Therefore, systematic investigation using an alternative theoretical approach is required to accurately describe CO_2 adsorption on the Cu surfaces.

To improve the description of weakly bound systems, Dion *et al.* developed the van der Waals density functional (vdW-DF) method, in which fully nonlocal correlation energy functional is introduced.[74–76] The exchange-correlation energy of the vdW-DF method is defined as the form of

$$E_{\mathrm{xc}}^{\mathrm{vdW}} = E_{\mathrm{x}}^{\mathrm{GGA}} + E_{\mathrm{c}}^{\mathrm{LDA}} + E_{\mathrm{c}}^{\mathrm{nl}}, \tag{3.1}$$

where $E_{\mathrm{x}}^{\mathrm{GGA}}$ and $E_{\mathrm{c}}^{\mathrm{LDA}}$ are GGA exchange energy and LDA correlation energy, respectively. The nonlocal correlation energy ($E_{\mathrm{c}}^{\mathrm{nl}}$) is described as

$$E_{\mathrm{c}}^{\mathrm{nl}} = \frac{1}{2} \int d^3r d^3r' n(\vec{r}) \phi(\vec{r}, \vec{r}') n(\vec{r}') \tag{3.2}$$

where $n(\vec{r})$ is the charge density and $\phi(\vec{r}, \vec{r}')$ is a kernel function described elsewhere.[74]

There have been countless applications of the vdW-DF method to a wide variety of systems. For instance, the original vdW-DF (vdW-DF1) was employed in solving CO adsorption puzzle on metal fcc (111) surfaces.[44] Furthermore, several modifications have been proposed to improve the accuracy of vdW-DF1. Lee *et al.* modified the exchange and nonlocal correlation parts of vdW-DF1 in the second version of the vdW functional, namely vdW-DF2, and demonstrated that it improves the equilibrium distances between non-covalently interacting molecules.[77] These vdW-DFs, however, tend to overestimate the lattice constants of solids and are not suitable for molecular adsorption on solid surfaces. Recently, several groups proposed more accurate vdW-DFs,[78–84] which successfully improve the description of molecules, solids, and adsorption systems.

3.2 Objectives

There are several studies of CO_2 adsorption and reaction on metal, metal-organic, and oxide surfaces with vdW corrections.[85–90] However, there is no systematic study of CO_2 adsorption on Cu surfaces using vdW-DFs. Hence, in this chapter, the adsorption of

CO_2 on the Cu surfaces was elucidated by using standard GGA with the Perdew-Burke-Ernzerhof (PBE) exchange-correlation functional[37] and a set of vdW-DFs, as well as the temperature programmed desorption (TPD) and X-ray photoelectron spectroscopy (XPS) experiments. Direct comparison between theoretical and experimental studies would give useful insight into appropriate vdW functionals for further investigation on related CO_2 activation on Cu surfaces.

3.3 Methods

3.3.1 Computational details

CO_2 adsorption on the flat Cu(111), stepped Cu(221), and kinked Cu(965) surfaces was studied to clarify the effect of the local surface geometry on the physisorbed state of CO_2. In this study, the results obtained using GGA-PBE exchange-correlation functional were compared with those using several vdW-DFs, *i.e.*, the original vdW-DF (vdW-DF1),[74,75] optB86b-vdW,[80] and rev-vdW-DF2[83] functionals. The dispersion correction proposed by Grimme for PBE (PBE-D2)[91] was also included.

The calculations were carried out by using STATE (Simulation Tool for Atom TEchnology) package, which previously has been applied in the synthesis of formate and its hydrogenation reaction,[13,69,92] CO_2 dissociation,[62] and benzene adsorption on Si(100).[93] The $(3 \times 2\sqrt{3})$ unit cell is used for Cu(111) with three layers thickness (the bottom atomic layer is fixed as its bulk positions). The dependence of the CO_2 adsorption energy on the size of the unit cells using (3×3) and (4×4), and slab thickness was also checked. The slab thickness was increased from three to six layers, in which the two bottom atomic layers are fixed at their bulk positions.

Based on Somorjai notation, the unit cell of Cu(221) is $(s \times 4)$, which covers one terrace and is expanded four times in the direction parallel to the step.[94] The similar unit cell of $(s \times 4)$ is also used to construct the kinked Cu(965) surface. The surface Brillouin zone is sampled by using a uniform grid of $4 \times 4 \times 1$ k-points for (3×3) and $(3 \times 2\sqrt{3})$ of Cu(111), $3 \times 3 \times 1$ k-points for (4×4) of Cu(111), and $3 \times 4 \times 1$ k-points for Cu(221) and Cu(965). The slab models were constructed based on the optimized Cu bulk lattice constant for each considered functionals. The distance between neighboring slabs in the direction perpendicular to the surface is more than 30 Å and it is enough to avoid undesired interaction.

The method developed by Wu and Gygi,[95] which is a simplified version of the Román-Pérez and Soler algorithm,[96] has been implemented for the nonlocal correlation energy and potential of vdW-DFs. The performance and accuracy of the method has been reported in Ref. 93. It suggested that the sufficient number of division of q_0 function in Wu and Gygi formulation (N_q) is 20. The electron-ion interaction was described by Vanderbilt's ultrasoft pseudopotentials[97]. The energy cutoffs of plane wave basis sets are 36 Ry and 400 Ry for wave function and charge density, respectively. The adsorption energy is converged within 1 kJ/mol with respect to the energy cutoffs.

At first, I assess the behavior of PBE, PBE-D2, and vdW-DFs in the CO_2 adsorption on Cu(111). The isolated CO_2 and clean Cu surfaces were optimized separately until the atomic forces became smaller than 8×10^{-2} nN (1×10^{-3} Hartree/Bohr). The isolated CO_2 and clean Cu surfaces were then combined. The interaction energy (E_{int}) of CO_2 on Cu(111) as a function of molecule-surface distance is defined by:

$$E_{\mathrm{int}} = E_{\mathrm{tot}} - (E_{\mathrm{surf}} + E_{\mathrm{CO_2}}) \tag{3.3}$$

where E_{tot}, E_{surf}, and $E_{\mathrm{CO_2}}$ represent the total energies of the adsorbed system, an isolated clean surface, and an isolated molecule in gas phase, respectively. After the equilibrium distance between CO_2 and surface was obtained, I again fully optimized the combined systems. The adsorption energy (E_{ads}) of CO_2 on the Cu surfaces is defined by the negative of E_{int} obtained at the fully relaxed geometry. The zero-point energy (ZPE) correction was included in the calculation of the most favorable adsorption site on the flat, stepped, and kinked Cu surfaces.

3.3.2 Experimental details

The TPD and XPS measurements were carried out in an ultra-high vacuum (UHV) chamber.[85,98] The base pressure was 1×10^{-10} Torr. The measurements were done on the Cu(111) surface, whereas the measurements on the stepped Cu surfaces had been reported previously.[60] The Cu(111) surface was cleaned with several cycles of Ne^+ ion sputtering and annealing at 673 K. Cleanness of the surface was checked by low-energy electron diffraction (LEED) and XPS. The temperature of the sample was measured by a K-type thermocouple attached to the side of the Cu crystal with a Ta foil. Temperature calibration in a low temperature region (<80 K) was conducted by TPD of Xe on Cu(111).[99,100] The sample was cooled by a continuous flow liquid He system (Advanced Research Systems, LT3B Helitran cryostat), and the minimum temperature of the Cu(111) crystal was 25 K in the present experiments. The CO_2 gas was introduced onto the surface by a pulse valve. In the TPD measurements, desorbing molecules were detected by a quadrupole mass spectrometer (QMS, Balzers QMS 200) with an apertured shield over the ionization source of QMS.[101] The XPS measurements were performed using an Al Kα X-ray (hν= 1486.6 eV) in the same UHV chamber using a hemispherical electron analyzer (VG Scienta, R3000) at a normal emission angle. CO_2 coverage was estimated from the area of its desorption peak and the intensity of its C 1s XPS peak. The C 1s peak intensity was calibrated by that of monolayer cyclohexane on Cu(111) ($\theta_{\mathrm{C_6H_{12}}} = 0.14$ ML).[102]

3.4 Results

3.4.1 CO_2 adsorption on Cu(111)

First, the Cu bulk lattice parameter was investigated by using PBE, PBE-D2, and set of vdW-DFs. As shown in Table 3.1, PBE and PBE-D2 slightly overestimate the Cu bulk lattice parameter.[80] The vdW-DF1 also overestimates the Cu bulk lattice parameter with larger deviation than PBE results. On the other hand, the Cu bulk lattice parameters obtained using rev-vdW-DF2 and optB86b-vdW are in good agreement with experimental value (3.615 Å).[103]

Table 3.1: Copper bulk lattice parameter (a) and its deviation (Δ) calculated using PBE, PBE-D2, and several vdW-DFs.

Functional	a / Å	Δ / %
PBE	3.642	0.76
PBE-D2	3.644	0.80
vdW-DF1	3.714	2.75
rev-vdW-DF2	3.617	0.06
optB86b-vdW	3.610	0.13
Expt.	3.615[a]	0.00

[a] Taken from Ref. 103.

Next, I investigated CO_2 adsorption on the flat Cu(111) surface. As shown in Fig. 3.1, I investigated the adsorption on the top, bridge, and two hollow sites. The interaction energy curves are shown in Fig. 3.2 and summarized in the Table 3.3. The considered functionals give strikingly different behavior for CO_2 adsorption on Cu(111). As shown in Fig. 3.2, PBE produces an almost repulsive interaction energy curve. Thus, the equilibrium distance between CO_2 and the surface is not well defined with PBE. On the other hand, the PBE-D2 and vdW-DFs are able to produce potential energy curve of CO_2 adsorption on Cu(111) with a clear equilibrium distance, being compatible with the general notion of atomic and/or molecular adsorption on solid surfaces.

As summarized in the Table 3.3, the adsorption energies of CO_2 on top, bridge, and hollow sites are quite similar, indicating that CO_2 is physisorbed on Cu(111). The equilibrium distance between Cu surface and CO_2 molecule is more than 3 Å. The CO_2 molecule is physisorbed with its molecular axis parallel to the Cu(111) surface at almost 180° of O$-$C$-$O bond angle and 1.18 Å of C$-$O bond length. The increase of the slab thickness from three to six does not affect the CO_2 adsorption energy.

The dependence of CO_2 adsorption energy on the unit cell size and energy cutoffs of plane wave basis sets were also checked. Here, the calculations was done using PBE-

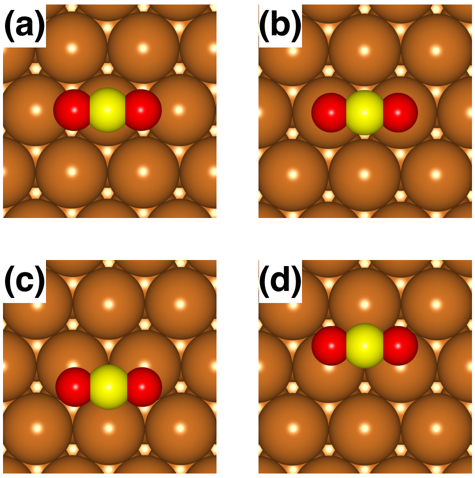

Figure 3.1: Top view of CO_2 adsorption on (a) top, (b) bridge, (c) fcc-hollow, and (d) hcp-hollow sites of Cu(111). The brown, yellow, and red balls correspond to the copper, carbon, and oxygen atoms.

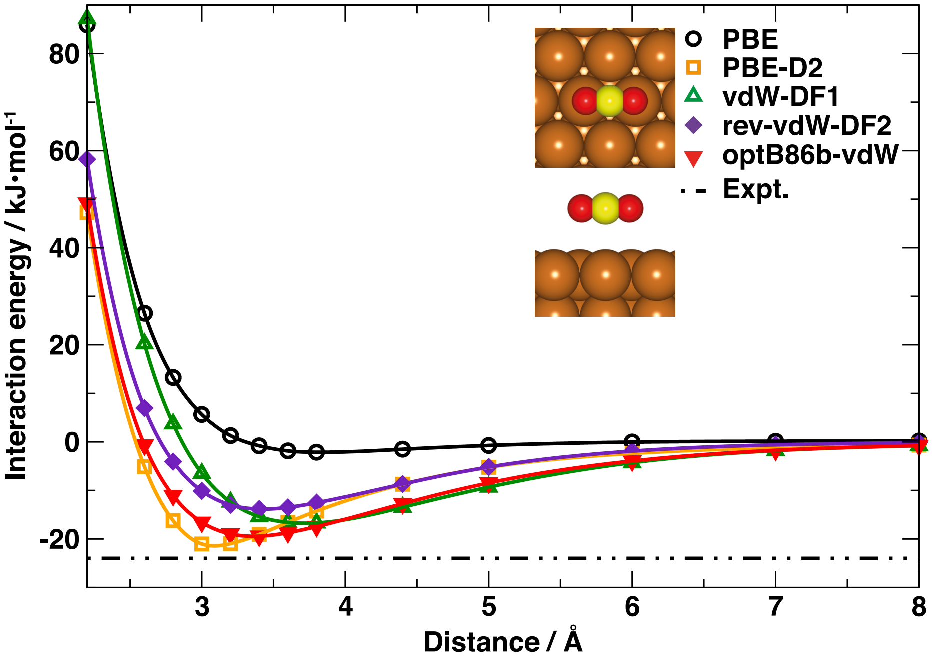

Figure 3.2: Interaction energy (E_{int}) curve of CO_2 on Cu(111) as a function of molecule-surface distance. Insets show top and side views of CO_2 adsorption on bridge site of Cu(111). The horizontal dashed-dotted line indicates the estimated desorption energy from TPD of CO_2 on Cu(111) at low coverage.

D2 and optB86b-vdW functionals since the calculated adsorption energies using these functionals are in rather good agreement with experimental results. As summarized in Table 3.2, the calculated CO_2 adsorption energy is changed less than 1 kJ/mol by varying the unit cell size and energy cutoffs. The calculated CO_2 adsorption energies are in the ranges of $21 - 22$ kJ/mol and $19 - 20$ kJ/mol using PBE-D2 and optB86b-vdW, respectively, and in good agreement with our measurement results.

Table 3.2: Calculated adsorption energy (E_{ads}) of CO_2 on Cu(111) using PBE-D2 and optB86b-vdW functionals with different unit cell size and energy cutoffs for the wave functions ($E_{\mathrm{cut}}^{\mathrm{wf}}$) and the augmented charge density ($E_{\mathrm{cut}}^{\mathrm{den}}$).

	E_{ads} / kJ $\cdot$ mol^{-1}	
	PBE-D2	optB86b-vdW
Unit cell size[a]		
(3×3)	22.34	20.00
$(3 \times 2\sqrt{3})$	21.48	19.63
(4×4)	22.32	19.70
$\mathbf{E_{cut}^{wf}; E_{cut}^{den}}$ / **Ry**[b]		
36; 400	21.48	19.63
36; 625	21.46	19.89
36; 900	21.51	19.10
64; 400	21.36	18.70
64; 625	21.31	19.07
64; 900	21.37	20.41

[a] Calculated using energy cutoffs of 36 Ry and 400 Ry for wave function and charge density.
[b] CO_2 adsorbs on $(3 \times 2\sqrt{3})$ of Cu(111).

Figure 3.3(a) shows a series of TPD spectra of CO_2 on Cu(111) as a function of exposure. In these measurements, CO_2 was adsorbed on the Cu(111) surface at 25 K, and TPD measurements of the as-deposited CO_2 layer were carried out with a heating rate of 1 K/s. At $\theta_{CO_2} < 0.02$ ML, single desorption peaks of CO_2 are observed at ~76 K with a desorption threshold temperature of 65 K. With increasing coverage, two desorption peaks are observed. The peak at lower and higher temperature may assign to the isolated CO_2 and crystalline CO_2 multilayer, respectively. It is noted that the CO_2 dissociative adsorption was not observed in the present TPD measurements on the Cu(111) surface. The similar assignment of this phenomenon was also reported previously.[60] Figure 3.3(b) shows the activation energies for desorption (E_{d}) as a function of coverage, which have been estimated by the threshold TPD method.[104,105] The desorption energies of CO_2 on Cu(111) at very low coverages are estimated to be $E_{\mathrm{d}} = {\sim}24$ kJ/mol. With increasing the coverage, the desorption energy of CO_2 slightly increases up to ~28 kJ/mol, and then it becomes 25 kJ/mol above ~0.04 ML, where the low-temperature leading edges become almost common. Note that this value is similar to that of multilayer CO_2 on graphene (25.4 kJ/mol) using the same measurement system.[85] Therefore, the strength of the substrate-molecule interaction on Cu(111) is comparable with the intermolecular interaction between condensed CO_2 molecules.

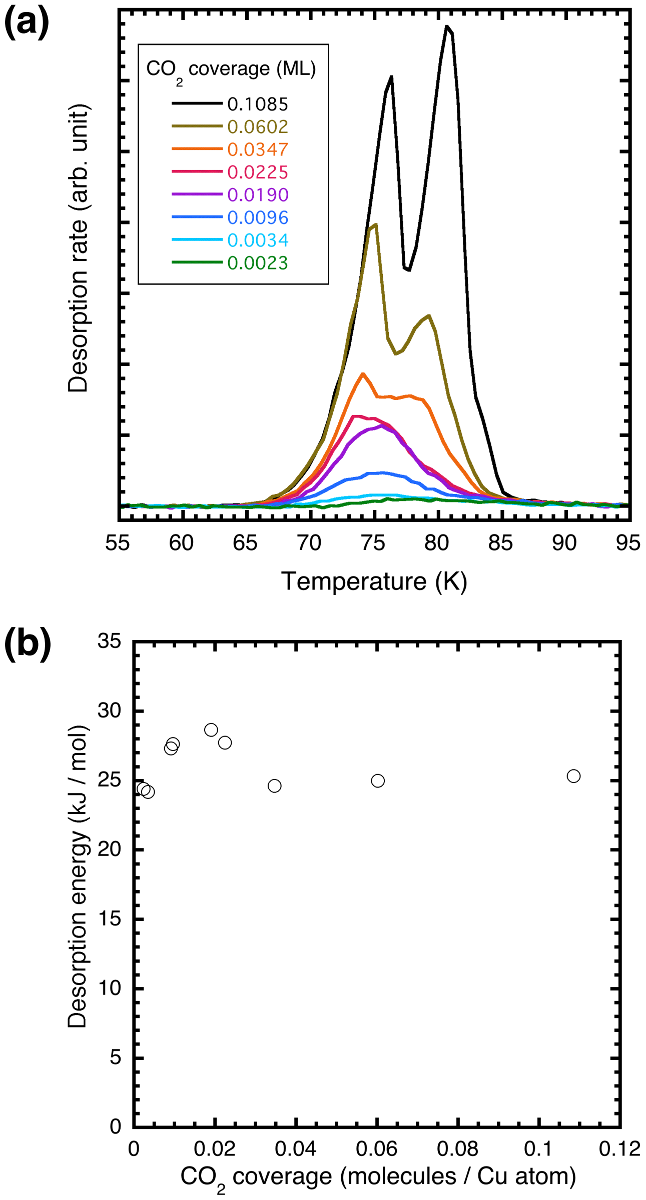

Figure 3.3: (a) A series of TPD spectra of CO_2 adsorbed on Cu(111) at 25 K as a function of coverage (44 amu/e). The heating rate is 1 K/s. (b) Estimated desorption energy of CO_2 adsorbed on Cu(111) as a function of coverage.

3.4.2 CO_2 adsorption on Cu(221) and Cu(965)

In this section, the CO_2 adsorption on stepped and kinked Cu surfaces was investigated. It has been shown in the previous subsection that the calculated adsorption energies by using PBE-D2 and optB86b-vdW functionals are in rather good agreement with experimental results. Thus, in the case of CO_2 adsorption on stepped and kinked Cu surfaces, I only focus in the calculations using optB86b-vdW functional. Figures 3.4 and 3.5 show possible CO_2 adsorption configurations near the step-edge and kink-edge, respectively. On Cu(221), the CO_2 is placed on the upper terrace with its molecular axis parallel and perpendicular to the step-edge [model (a)-(d) in Fig. 3.4]. The molecule is also put on the lower terrace with its molecular axis parallel to the step-edge [model (e) in Fig. 3.4]. In the case of model (e), the most stable position was determined in two dimensional parameter [y-z plane] as shown in the schematic of Fig. 3.4(f). The calculated adsorption energy of each configuration is shown within the figure.

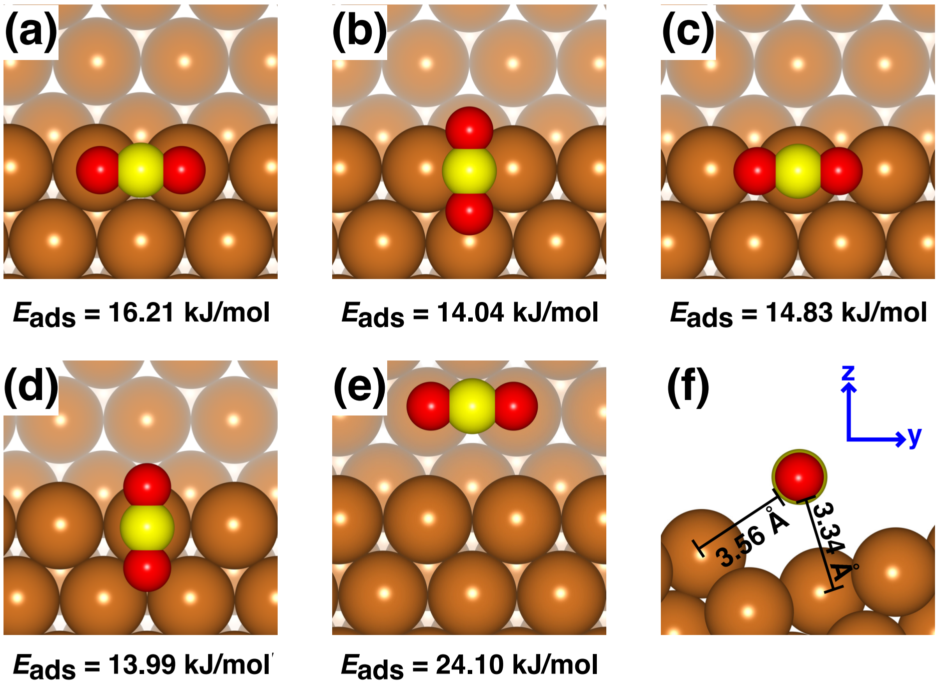

Figure 3.4: Adsorption configurations of CO_2 on the stepped Cu(221) surface: on the bridge site of the upper terrace with its molecular axis (a) parallel and (b) perpendicular to the step-edge, on the top site of the upper terrace with its molecular axis (c) parallel and (d) perpendicular to the step-edge, and (e) on the bridge site of the lower terrace with its molecular axis parallel to the step-edge. (f) Side view of CO_2 adsorption in model (e). The calculations were done by using optB86b-vdW functional.

Based on the calculation results, model (e) is the most stable configuration of CO_2 on the stepped Cu surface. As shown in the Fig. 3.4(f), CO_2 is located 3.56 from the step-edge row and 3.34 from the lower terrace area of the surface. The CO_2 adsorption energy in this model is 24.10 kJ/mol, which is more stable than that of other models

Table 3.3: Adsorption energy of CO_2 on Cu(111) (E_{ads}), CO_2-surface distance $d_{\mathrm{CO_2-Cu}}$, C−O bond length ($l_{\mathrm{C-O}}$) and O−C−O bond angle ($\angle_{\mathrm{O-C-O}}$) obtained with PBE, PBE-D2, and several vdW-DFs. CO_2 adsorption energies on six layers Cu(111) are put in the square bracket.

Functional		Adsorption sites			
		top	bridge	fcc	hcp
PBE	E_{ads} / kJ · mol^{-1}	2.24	2.10	2.12	2.12
	$d_{\mathrm{CO_2-Cu}}$ / Å	3.95	3.83	3.87	3.85
	$l_{\mathrm{C-O}}$ / Å	1.18	1.18	1.18	1.18
	$\angle_{\mathrm{O-C-O}}$ / deg.	179.92	180.00	180.00	180.00
PBE-D2	E_{ads} / kJ · mol^{-1}	19.50	21.48 [22.55]	21.16	21.23
	$d_{\mathrm{CO_2-Cu}}$ / Å	3.18	3.09	3.07	3.06
	$l_{\mathrm{C-O}}$ / Å	1.18	1.18	1.18	1.18
	$\angle_{\mathrm{O-C-O}}$ / deg.	179.50	179.89	179.88	179.76
vdW-DF1	E_{ads} / kJ · mol^{-1}	16.29	16.75	16.41	16.41
	$d_{\mathrm{CO_2-Cu}}$ / Å	3.78	3.68	3.74	3.74
	$l_{\mathrm{C-O}}$ / Å	1.18	1.18	1.18	1.18
	$\angle_{\mathrm{O-C-O}}$ / deg.	179.89	179.97	179.98	179.98
rev-vdW-DF2	E_{ads} / kJ · mol^{-1}	13.15	14.10	13.90	13.92
	$d_{\mathrm{CO_2-Cu}}$ / Å	3.54	3.29	3.35	3.36
	$l_{\mathrm{C-O}}$ / Å	1.18	1.18	1.18	1.18
	$\angle_{\mathrm{O-C-O}}$ / deg.	179.79	179.99	179.91	179.91
optB86b-vdW	E_{ads} / kJ · mol^{-1}	18.68 [18.07]	19.63 [19.37]	19.61 [18.95]	19.63 [18.97]
	$d_{\mathrm{CO_2-Cu}}$ / Å	3.48 [3.46]	3.29 [3.29]	3.29 [3.28]	3.29 [3.28]
	$l_{\mathrm{C-O}}$ / Å	1.18 [1.18]	1.18 [1.18]	1.18 [1.18]	1.18 [1.18]
	$\angle_{\mathrm{O-C-O}}$ / deg.	179.73 [179.89]	179.99 [179.99]	179.90 [179.99]	179.88 [179.99]
Expt. works[a]	E_{ads} / kJ · mol^{-1}	24			

[a] Measured activation energy for desorption of CO_2 on Cu(111) adsorbed at 25 K.

by about 10 kJ/mol. The CO_2 adsorption energy on the stepped Cu surface is more stable than on the flat Cu surface by about 5 kJ/mol.

Next, the CO_2 adsorption on the kinked Cu surface was investigated. Here, the CO_2 is placed on the lower terrace with its molecular axis parallel to the step-edge and kink-edge of Cu(965) (shown in Fig. 3.5). At the step-edge area [model (a)-(c)], the CO_2 adsorption was optimized starting from the geometry of the most stable adsorption state on the stepped Cu(221) surface. Near the kink-edge [model (d)], the CO_2 was aligned with its molecular axis rotated 30° with respect to the step-edge. Then, the favorable position is traced with respect to the distance between CO_2 and second layer surface, and the kink-edge atoms. The calculation results show that model (d) is the most stable configuration. The adsorption energy of CO_2 in this model is 26.12 kJ/mol, which is more stable than on a pure stepped Cu surface by about 2 kJ/mol. The CO_2 is located 3.79 Å from the lower terrace, where the distance of the two oxygen atoms from the step-edge and kinked-edge atoms are 2.87 Å and 2.92 Å, respectively (Fig. 3.5d).

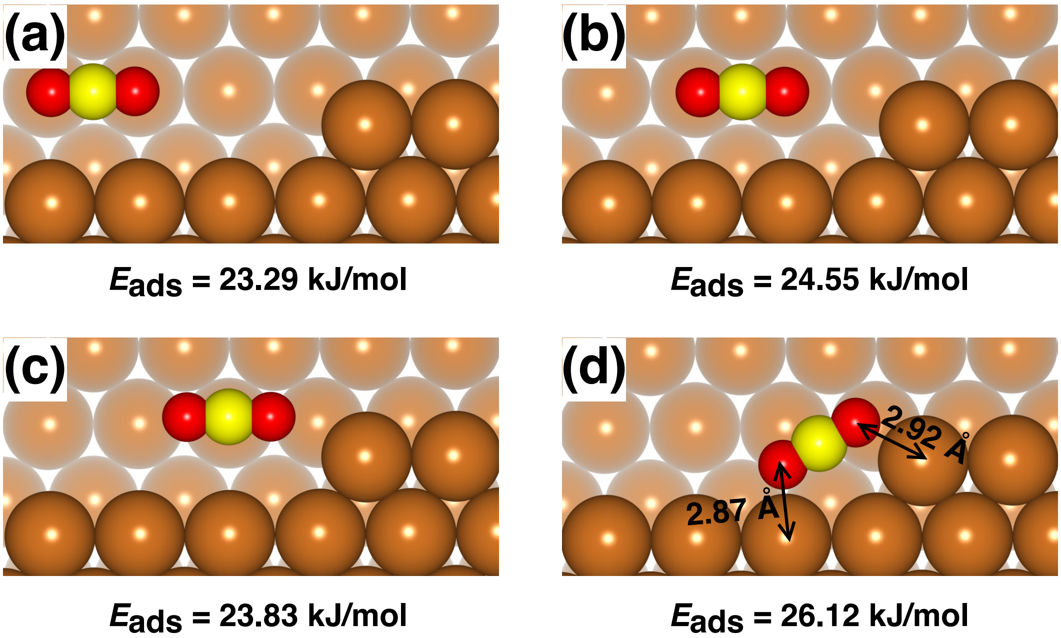

Figure 3.5: CO_2 adsorption configurations on the kinked Cu(965) surface: (a) - (c) CO_2 is located on the lower terrace with its molecular axis parallel to the step-edge, and (d) with its molecular axis rotated by 30° with respect to the step-edge. The calculations were done by using optB86b-vdW functional.

3.5 Discussion

First, the TPD spectra of CO_2 desorption from Cu(111) is discussed. At very low coverage (0.0023 ML), the desorption peak is located at ∼80 K (shown in Fig 3.3(a)). The desorption peak is then shifted to the lower temperature (∼76 K) as coverage increasing. The shifting of desorption peaks is not only due to the desorption energy, but also pre-exponential factor. The pre-exponential factor at very low coverage is probably smaller than those at higher coverages. At above 0.02 ML two main desorption peaks were observed. The peaks are located at 74 K and 78 K, 75 K and 79 K, 76 K and 81 K for 0.0347 ML, 0.0602 ML, and 0.1085 ML, respectively. These peaks may correspond to the desorption of multilayer and/or 2-dimensional-condensed CO_2.

The CO_2 adsorption energies on the flat, stepped, and kinked Cu surfaces as well as the measured adsorption energies are summerized in Table 3.4. The calculated CO_2 adsorption energy on Cu(111) is 19 kJ/mol and insensitive to the coverage and slab thickness. Relative to Cu(111), the CO_2 adsorption energies increase about 5 kJ/mol and 7 kJ/mol on the stepped and kinked Cu surfaces, respectively. The ZPE correction was also considered in the adsorption energy calculation using the presented vibrational frequencies data in the Table 2.3. The calculated adsorption energies change only by 1 kJ/mol by including the ZPE correction. The adsorption energy of CO_2 on Cu(111) is $19 - 21$ kJ/mol based on PBE-D2 and optB86b-vdW calculation results, which agrees reasonably well with the experimental value of 24 kJ/mol. However, the calculated adsorption energies are systematically underestimated by $3 - 5$ kJ/mol compared with the measured value at very low coverage. There are two possible origins for the discrepancy. First, CO_2 may adsorb on the stepped edge area of Cu(111) at very low coverage since the calculated CO_2 adsorption energy on Cu(221) (24.10 kJ/mol) is quite similar with the measured value. Secondly, CO_2 may aggregate at even very low coverage and may be stabilized to increase the adsorption energy. In the previous TPD study, it was shown that the pre-annealing induces higher desorption temperature of CO_2 indicating attractive intermolecular interaction among the neighboring CO_2 molecules.[60] Since there is only small density of the stepped edges on Cu(111) in the experimental sample, the aggregation of CO_2 may be more plausible for the origin of the larger adsorption energy measured by TPD experiments.

As shown in Table 3.4, the calculated asymmetric modes of physisorbed CO_2 on the flat, stepped, and kinked Cu surfaces are 2362 cm^{-1}, 2352 cm^{-1}, and 2349 cm^{-1}, respectively. They differ from the gas phase value (2385 cm^{-1}) by 23 cm^{-1}, 33 cm^{-1}, and 36 cm^{-1} for flat, stepped, and kinked Cu surfaces, respectively. On the other hand, experimentally observed CO_2 asymmetric mode on the terrace (step) area of Cu(997)[60] are 6−12 cm^{-1} (29 cm^{-1}) lower than that of gas phase asymmetric mode of CO_2.[106] Based on these vibrational frequencies difference, several CO_2 adsorption states on the Cu surfaces can be clarified.

3.6 Summaries

The CO_2 adsorption on Cu surface was studied by means of DFT as well as TPD and XPS measurements. The considered functionals give different behaviors in describing CO_2 adsorption potential on Cu surfaces. The standard PBE produces an almost repulsive potential energy curve for CO_2 adsorption on the flat Cu surface, whereas PBE-D2 and vdW-DFs give deeper potential energy curves. The vdw-DF1 and rev-vdW-DF2 slightly underestimate CO_2 adsorption energy, whereas PBE-D2 and optB86b-vdW give better agreement with the TPD results. The calculated CO_2 adsorption energies using optB86b-vdW functional on the Cu(111), Cu(221) and Cu(965) surfaces are in the range of $20 - 27$ kJ/mol. On the stepped and kinked Cu surfaces, CO_2 prefers to adsorb on the lower terrace with its molecular axis parallel to the step-edge and in tilted alignment near the kink site, respectively. The calculated CO_2 adsorption energy on Cu(111) is still underestimated by $3 - 5$ kJ/mol compared with the measured value of 24 kJ/mol at very low coverage. This discrepancy may be due to the aggregation of CO_2 at low coverage, which can lead to the stabilization of adsorbed molecules through the attractive intermolecular interaction. The present results provide valuable insight to consider the appropriate exchange-correlation functional for further theoretical study in the adsorption/activation and reduction of CO_2 on the surfaces of heterogeneous catalysts.

Table 3.4: Calculated and measured CO_2 adsorption energy (E_{ads}) on the flat, stepped, and kinked Cu surfaces, and vibrational frequencies of gas phase and physisorbed CO_2 on its preferred adsorption sites. The adsorption energies on six layers slab surface and with ZPE correction are put in the italic and square bracket, respectively. The calculations were done by using the optB86b-vdW functional.

	E_{ads} / $\text{kJ} \cdot \text{mol}^{-1}$				Frequencies / cm^{-1}	
	Theory		Experiment			
	This works	Prev. works	This works	Prev. works	This works[a]	Prev. works[b]
CO_2 gas	–	–	–	–	618, 619, 1328, 2385	2349[c]
Cu(111)	19.63; *19.37* [19.04]; [*18.77*]	7.72[d], 20.26[f]	24	20.91[e]	18, 59, 83, 587, 605, 1321, 2362	2453[d]
Cu(221)	24.10; *24.00* [23.56]; [*23.47*]	–	–	–	56, 60, 91, 577, 593, 1290, 2352	–
Cu(997)[g]	–	–	–	20.6[h], 24.6[j]	–	2337[i], 2343[i], 2325[k]
Cu(965)	26.12; *26.60* [25.62]; [*26.11*]	–	–	–	47, 71, 91, 565, 589, 1307, 2349	–

[a] Theoretical calculations.

[b] Asymmetric mode of CO_2.

[c] Experimental value taken from Ref. 106.

[d] Calculated value using GGA-PW91 functional (Ref. 11).

[e] Experimental value taken from Ref. 107.

[f] Calculated value using PBE-D2 functional (Ref. 89).

[g] Taken from Ref. 60.

[h] Measured adsorption energy for as-deposited CO_2 using the threshold TPD method.

[i] Measured frequencies from the terrace area of Cu(997).

[j] Measured adsorption energy for pre-annealed CO_2 using the threshold TPD method.

[k] Measured frequency from the step area of Cu(997).

Chapter 4

Desorption Dynamics of CO_2 from Formate Decomposition on the Cu(111) Surface

4.1 Background

One of the most important intermediate steps in the methanol synthesis over Cu-based catalysts is CO_2 hydrogenation into formate (HCOO).[8–12] Based on a kinetics analysis, it was clarified that formate synthesis is structure insensitive and consistent with an Eley-Rideal (ER) type mechanism.[13–16] The ER type mechanism suggests that the formate synthesis can be enhanced by controlling the translational, vibrational, and rotational energies of impinging CO_2. The initial impinging CO_2 energies must be related to the energy states of desorbed CO_2 from formate decomposition because formate synthesis and decomposition are reverse reactions. Therefore, elucidation of formate decomposition dynamics is important for improving catalytic formate synthesis.

Very recently, the dynamics of desorbed CO_2 produced from the formate decomposition reaction has been studied by measuring the angle-resolved intensity and translational energy distribution of the steady-state reaction of formic acid (HCOOH) and oxygen on a Cu surface.[108] It was reported that the translational energy of desorbed CO_2 is approximately 0.10 eV and independent of the surface temperature. The measured CO_2 translational energy is much smaller than the activation energy of formate synthesis, which is 0.59 ± 0.05 eV.[14–16] This suggests that internal modes, such as vibrational and rotational modes, should be excited in the desorbed CO_2.

4.2 Objectives

In this study, the energy distribution of desorbed CO_2 as a formate decomposition product (Fig. 4.1) was elucidated by means of *ab initio* calculations. Here, the importance of the van der Waals (vdW) interaction in determining the energetics of desorbed CO_2 was also shown. From knowledge of desorbing product dynamics, we can deduce optimal conditions for the formate synthesis reaction through CO_2 hydrogenation.

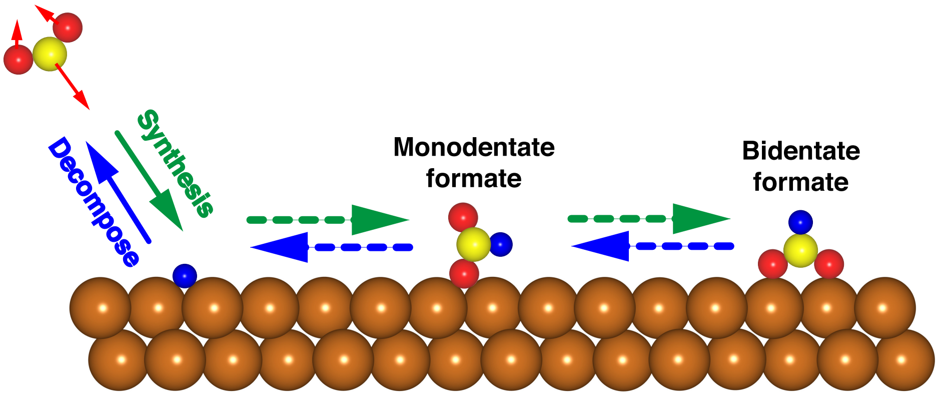

Figure 4.1: Schematics of formate synthesis and decomposition on Cu(111).

4.3 Computational details

The calculations were performed using the STATE code, which previously has been used for formate adsorption,[69] formate hydrogenation,[92] CO_2 hydrogenation,[13] CO_2 dissociation,[62] and *ab initio* molecular dynamics (AIMD) study of methanol electrooxidation.[109] I compared the results obtained using the Perdew-Burke-Ernzerhof (PBE)[37] functional with those using several vdW density functionals (vdW-DFs), *i.e.*, the original vdW-DF (vdW-DF1),[74,75] optB86b-vdW,[80] and rev-vdW-DF2[83] functionals. I also included the dispersion correction proposed by Grimme with PBE (PBE-D2).[91] The implementation of the self-consistent vdW-DF[95,96,110] in the STATE code is described in Ref. 93. The cutoff energies of 36 and 400 Ry were used for the wave functions and the augmented charge density, respectively. The electron-ion interaction was described using Vanderbilt's ultrasoft pseudopotentials.[97] The Cu(111) surface was modeled using a three layer-thick (3×3) unit cell with the bottommost atomic layer fixed to its bulk configuration. The distance between the two neighboring slabs is more than 30 Å. The surface Brillouin zone was sampled using a uniform grid of $4 \times 4 \times 1$ k-points. The climbing image nudged elastic band method[111,112] was used to obtain the minimum energy path, the transition state (TS), and the activation energies of formate synthesis from CO_2 hydrogenation. The vibrational frequencies of the adsorbed species at the TS is calculated using the frozen phonon approximation. One imaginary frequency was obtained in the TS structure, which indicated that the geometry was a first-order saddle point on the potential energy curve. Starting from the TS structure, the AIMD simulations were performed to evaluate the translational and internal (rotational and vibrational) energies of desorbed CO_2 from the Cu surface. In these simulations, the initial velocities are given randomly and they are scaled to make the average kinetic energy of 300 K. The additional samples of initial geometry for AIMD simulations were also considered. In order to provide additional initial geometries, I displaced the atoms at TS towards the second, third, fourth, fifth, and sixth lowest normal mode vectors in such a way that the energies of the displaced geometries increased from the energy of TS by 0.02 eV (detailed results are presented in the Appendix). Moreover, the zero-point energy is not included in the sampling of initial conditions. Then, the system was evolved without velocity scaling or thermostat.

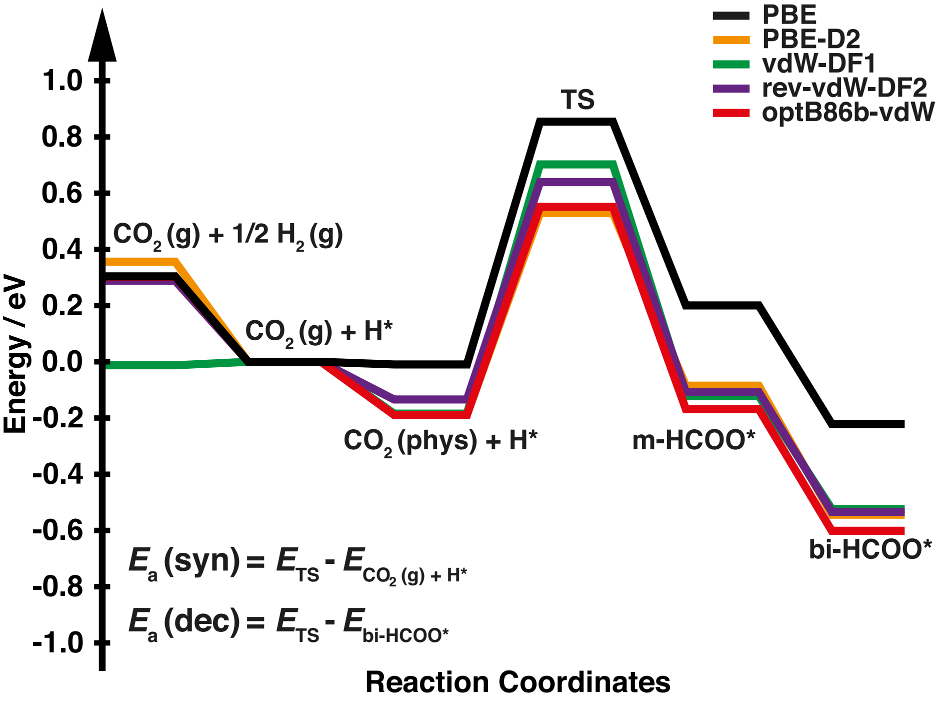

Figure 4.2: Energy profile for CO_2 hydrogenation to bidentate formate on Cu(111). The energy zero is the sum of the total energies of gas phase CO_2 and an adsorbed hydrogen on the surface (CO_2 (g) + H*).

4.4 Results

4.4.1 CO_2 hydrogenation into formate

First, the minimum energy path of CO_2 hydrogenation to bidentate formate (bi-HCOO) through monodentate formate (m-HCOO) on Cu(111) was calculated. The bidentate formate has been observed experimentally as an abundant product during CO_2 hydrogenation compared with its isomer (hydrocarboxyl (HOCO)).[14–16] Moreover, I have also performed the calculations of HOCO adsorption on Cu(111) and found that this species is 0.89 eV less stable using optB86b-vdW functional. Figure 4.2 and Table 4.1 show the energy profile for CO_2 hydrogenation into formate and its detailed descriptions, respectively. As shown in Fig. 4.2, the hydrogen chemisorption energies (the energy levels of CO_2 (g) + 1/2 H_2(g)) are quite similar among all functionals except vdW-DF1. On the other hand, the physisorption energies of CO_2 (the energy levels of CO_2 (phys) + H^*), the energies of the TSs, m-HCOO*, and bi-HCOO* are stabilized through the vdW attraction by approximately 0.13−0.37 eV relative to the PBE result. The activation energy of formate synthesis (E_a(syn)) is considered as the energy difference between the TS and the CO_2 (g) + H^* state. This definition of E_a(syn) should correspond to the experimentally observed activation energy of formate synthesis, in which formate was synthesized at a temperature of 333−353 K under atmospheric pressure.[14] In these conditions, the hydrogen coverage is close to the saturation point, while CO_2 coverage is almost negligible due to a small adsorption energy. The activation energy of formate decomposition (E_a(dec)) is defined as the energy difference between the TS and the bi-HCOO*. As shown in Table 4.1, only PBE overestimates the experimental E_a(syn), while each functional with a vdW interaction gives a reasonably good result. Meanwhile, each calculated E_a(dec) is in good agreement with the experimental results.

4.4.2 CO_2 translational energy

Next, I explored the energy distribution of desorbed CO_2 as a product of formate decomposition. The CO_2 translational energy (E_t) was calculated from the velocity of the center of mass of CO_2 (v_COM):

$$E_\mathrm{t} = \frac{1}{2} m_{\mathrm{CO_2}} \sum v_{\mathrm{COM}}^2 \tag{4.1}$$

Figure 4.3a summarizes the time evolution of CO_2 translational energy. The representative snapshots of CO_2 desorption from the AIMD trajectory are shown in Fig. 4.3b. There are significant differences in the E_t profiles calculated using PBE and those using PBE-D2 and vdW-DFs. Here, PBE predicts constant E_t at 0.30 eV after the CO_2 molecule experiences Pauli repulsion in the first 0.10 ps (shown as a black line in Fig. 4.3a). Meanwhile, the PBE-D2 and vdW-DFs show different time evolution profiles of CO_2 translational energy. In the first 0.08−0.10 ps, the E_t increases to 0.20−0.32 eV due to the Pauli repulsion between CO_2 and the surface. Then, it decreases gradually to a certain value due to the vdW attraction between CO_2 and the Cu(111) surface. These E_t pofiles are proportional to the potential energy surface of CO_2 adsorption on Cu(111) (shown in Fig. 3.2), in which PBE fails to describe the potential energy curve of CO_2 on Cu(111) while PBE-D2 and vdW-DFs are able to produce potential energy curve of CO_2 adsorption on Cu(111) with a clear equilibrium distance. The desorption angle (β) of CO_2 was estimated at 0.68 ps, when CO_2 already has constant E_t, from the direction of the velocity of center of mass relative to the surface normal (Fig. 4.3b). The calculated β using PBE, PBE-D2, vdW-DF1, rev-vdW-DF2, and optB86b-vdW are 5°, 18°, 8°, 12°, and 14°, respectively, in which the angular distribution of desorbed CO_2 shows quite sharp collimation along the surface normal direction and is in good agreement with experimental results.[108] As summarized in Table 4.2, the calculated E_t using PBE-D2 and vdW-DFs are in reasonable agreement with the experimental estimation,[108] while PBE fails in predicting this energy. Therefore, the vdW interaction is important for describing the translational energy of desorbed CO_2.

Table 4.1: Detailed descriptions of the energy profile of CO_2 hydrogenation into formate (in eV) on Cu(111), and calculated formate synthesis and decomposition energies using PBE, PBE-D2, and vdW-DFs. The values in brackets were obtained using a six layer-thick slab. The zero-point energy (ZPE) correction is evaluated by using optB86b-vdW functional.

	This study					Expt.
	PBE	PBE-D2	vdW-DF1	rev-vdW-DF2	optB86b-vdW	
$E_{\mathrm{CO_2(g)+1/2H_2(g)}}$	+0.30 (+0.22)	+0.36	−0.01	+0.29	+0.30 (+0.22)	–
$E_{\mathrm{CO_2(phys)+H^*}}$	−0.01 (−0.01)	−0.19	−0.18	−0.13	−0.19 (−0.18)	–
E_{TS}	+0.85 (+0.78)	+0.53	+0.70	+0.64	+0.55 (+0.52)	–
$E_{\mathrm{m\text{-}HCOO^*}}$	+0.20 (+0.17)	−0.08	−0.12	−0.11	−0.17 (−0.18)	–
$E_{\mathrm{bi\text{-}HCOO^*}}$	−0.22 (−0.33)	−0.54	−0.52	−0.53	−0.60 (−0.70)	–
E_{a}(syn)	0.85 (0.78)	0.53	0.70	0.64	0.55 (0.52)	
E_{a}(syn) + ZPE	0.80 (0.73)	0.48	0.65	0.59	0.50 (0.47)	0.59 ± 0.05[a] 0.66 ± 0.02[b]
E_{a}(dec)	1.08 (1.12)	1.07	1.23	1.17	1.15 (1.22)	
E_{a}(dec) + ZPE	0.90 (0.94)	0.89	1.05	0.99	0.97 (1.04)	1.12 ± 0.03[a] 1.17 ± 0.13[b]

[a] Taken from Ref. 14.

[b] Taken from Ref. 15 and 16.

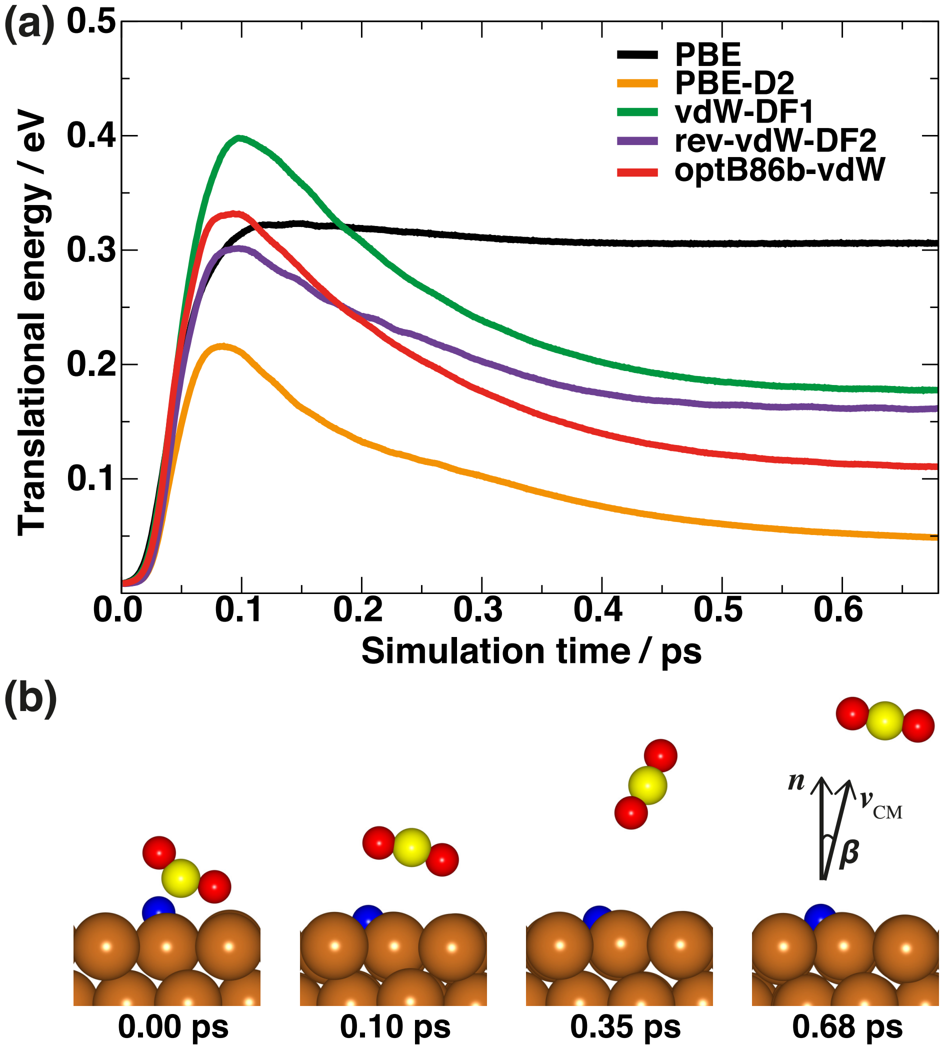

Figure 4.3: (a) Time evolution of the translational energy of desorbed CO_2 from formate decomposition calculated using PBE, PBE-D2, and vdW-DFs. (b) Representative snapshots from AIMD trajectory of CO_2 desorption. The $\boldsymbol{n}$ and $\boldsymbol{v}_{\mathrm{CM}}$ represent the direction of the surface normal and the velocity of center of mass of CO_2, respectively.

Table 4.2: Calculated translational energy (E_t), rotational energy (E_r), vibrational energy of bending mode (E_b), and vibrational energy of symmetric stretching mode (E_s) of desorbed CO_2 from formate decomposition on Cu(111) using PBE, PBE-D2, and vdW-DFs (in eV). The calculation results using optB86b-vdW functional are the average results from several samples of AIMD trajectory.

	This study					Expt.[a]
	PBE	PBE-D2	vdW-DF1	rev-vdW-DF2	optB86b-vdW	
E_t	0.30	0.05	0.18	0.16	0.14 ± 0.03	0.10
E_r	0.08	0.09	0.08	0.11	0.11 ± 0.03	–
E_b	0.27	0.24	0.25	0.26	0.26 ± 0.02	–
E_s	0.06	0.05	0.10	0.08	0.04 ± 0.02	–
Surface mode[b]	0.14	0.10	0.09	0.03	0.03 ± 0.02	–

[a] Experimentally measured CO_2 translational energy as a formate decomposition product taken from Ref. 108.

[b] This energy is deduced from the following: $E_\mathrm{a}(\mathrm{syn}) - (E_\mathrm{t} + E_\mathrm{r} + E_\mathrm{b} + E_\mathrm{s})$.

4.4.3 CO_2 internal energies

I also evaluated the energy transfer by formate decomposition into the internal modes (rotational and vibrational) of CO_2. The rotational energy (E_r) of CO_2 was estimated from the moment of inertia of CO_2 (I) and its angular momentum (L) at each time step of the AIMD trajectory:

$$E_\mathrm{r} = \frac{1}{2} \sum L_\mathrm{i} I_\mathrm{ij}^{-1} L_\mathrm{j} \tag{4.2}$$

Table 4.2 shows that the calculated E_r varies in between 0.08−0.11 eV.

The CO_2 bending, symmetric stretching, antisymmetric stretching vibrational energies are evaluated based on the time evolution of the desorbed CO_2 geometry, *i.e.*, bond angle (θ), the C−O bond length (l), and the difference between two C−O bond lengths (Δ), respectively, as shown in Fig. 4.4. For the comparison, the vibrational frequencies of an isolated CO_2 was also evaluated. The calculated zero-point energies of isolated CO_2 bending, symmetric stretching, and antisymmetric stretching vibrational modes are shown in Table 4.3. These calculated zero-point energies are nearly independent of the functional.

The energy of each vibrational mode of desorbed CO_2 was estimated by fitting them into the database of the relative stability of isolated CO_2 as a function of the θ, l, and Δ (shown in Fig. 4.5). For an example, the amplitude of the CO_2 bond angle in one period is between 160.6° and 199.4° as shown in the top panel of Fig. 4.4. If we fit this

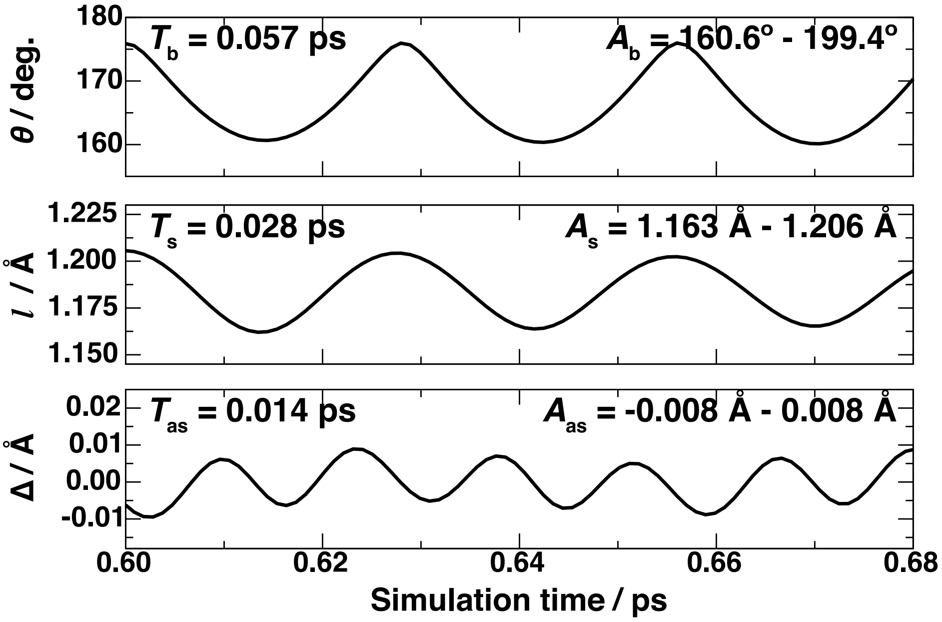

Figure 4.4: Time evolution of the CO_2 bond angle (θ), the C−O bond length (l), and the difference between two C−O bond lengths (Δ) based on AIMD trajectory calculated using optB86b-vdW functional. The period (T) and amplitude (A) of each geometry data are shown in each panel.

Table 4.3: Calculated vibrational frequencies of bending (ν_b), symmetric stretching (ν_s), antisymmetric stretching (ν_{as}) modes, and C−O bond length (l) of isolated CO_2 using PBE, PBE-D2, and vdW-DFs. The frequency and bond length are in meV and Å, respectively.

	This study					Expt.
	PBE	PBE-D2	vdW-DF1	rev-vdW-DF2	optB86b-vdW	
ν_b	77.34	77.59	76.19	76.58	76.72	82.70[a]
ν_s	164.91	164.47	162.78	164.48	164.61	165.27[b]
ν_{as}	296.83	296.11	291.38	295.14	295.74	291.24[b]
l	1.179	1.180	1.182	1.179	1.179	1.162[c]

[a] Taken from Ref. 113.
[b] Taken from Ref. 106.
[c] Taken from Ref. 114.

value to the data for the relative stability of isolated CO_2, it shows that desorbed CO_2 has a bending mode energy (E_b) of approximately 0.25 eV. This E_b is close to the third excitation of zero-point energy of isolated CO_2. All functionals produce similar E_b in the range of $0.24-0.26$ eV. The calculated vibrational energy of the CO_2 symmetric mode (E_s) varies between $0.05 - 0.11$ eV, which is close to the zero-point energy of the isolated CO_2 symmetric mode. Meanwhile, the vibrational energy of the antisymmetric mode ($E_\mathrm{as} \sim 1.5$ meV) is much smaller than the zero-point energy of isolated CO_2.

4.5 Discussions

Based on the calculation results, nearly a half of the E_a(syn) is transferred into CO_2 bending mode, a quarter into each translational and rotational modes, and rather small energy is transferred into CO_2 stretching modes. The origin for the strong enhancement of the CO_2 bending mode can be ascribed to its geometry at the TS, in which CO_2 bond angle is nearly 140°. The rest of E_a(syn) may transfer into the surface modes, namely, hydrogen$-$Cu and/or Cu$-$Cu vibrations. In order to clarify the present calculation results, I also performed the sudden vector projection (SVP) analysis proposed by Jiang and Guo.[115] In this analysis, the collision between reactants is assumed to be an instantaneous event, in which is appropriate at high collision energies. Thus, the CO_2 does not have enough time to change its internal state when it collides with adsorbed hydrogen. As a result, the reactivity for CO_2 in a particular vibrational state (v) is proportional to the overlap between its vibrational wave function and the wave function at the transition state

$$P_v \propto \langle \psi_v | \psi_\mathrm{TS} \rangle. \tag{4.3}$$

Instead of calculating the quantum overlap described in Eq. 4.3, the relative efficacy of a particular motion of CO_2 can be estimated by the projection of its normal mode vector onto the vector representing the reaction coordinate (s), such as the eigenvector with an imaginary frequency at the TS

$$\langle \psi_v | \psi_\mathrm{TS} \rangle \approx \vec{Q}(v) \cdot \vec{Q}(s). \tag{4.4}$$

The SVP analysis qualitatively agrees rather well with present AIMD simulation results. Based on the SVP analysis (shown in the Table 4.4), the CO_2 bending mode has second larger projection value compare with its translational, symmetric and antisymmetric stretching modes. It indicates that the bending mode of desorbed CO_2 is excited during the decomposition process. The SVP analysis also shows that the ki-

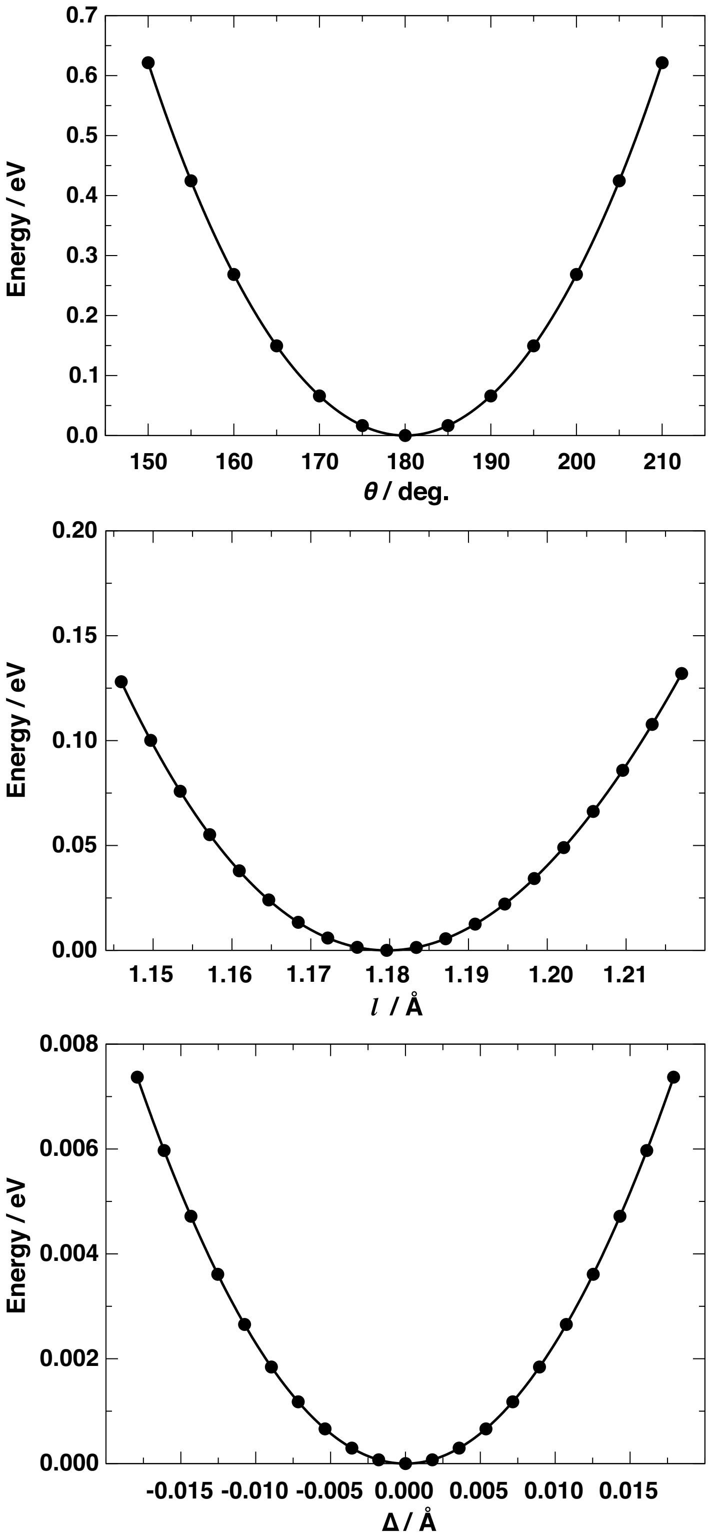

Figure 4.5: Relative stability of an isolated CO_2 molecule with respect to its bond angle (θ), the C−O bond length (l), and the difference between two C−O bond lengths (Δ).

Table 4.4: Comparison of the projection values of the translational and vibrational modes of CO_2 and H atom onto the CO_2 hydrogenation reaction modes at TS.

	SVP value
CO_2-translation	0.12
CO_2-bending	0.27
CO_2-symmetric	0.04
CO_2-antisymmetric	0.02
H-translation	0.79

netic mode of adsorbed hydrogen has the largest projection value. The large projection value of kinetic mode of hydrogen atom might be due to its displacement with respect to the surface. Hydrogen atom is easier to move since it has smaller mass compare with CO_2 molecule. However, this does not indicate that excitation of adsorbed hydrogen will enhance formate synthesis. It is because the transferred energy into the surface mode is quite small as shown in the Table 4.2. Therefore, the molecular dynamics analysis is necessary to elucidate the excited modes of desorbed CO_2.

The present results are in sharp contrast to the case of CO_2 dissociation, in which the CO_2 symmetric and antisymmetric stretching modes are theoretically suggested to be more important to increase the dissociation rate.[116] The importance of stretching modes in the CO_2 dissociation was implied experimentally in the study of CO_2 dynamics from CO oxidation on Pd surfaces.[117–120] The desorbed CO_2 has 0.12−0.16 eV in the vibrational energy of antisymmetric mode, which is slightly larger than the vibrational energy of CO_2 symmetric-bending mode (0.11−0.13 eV). Moreover, the measured translational (0.10−0.12 eV)[121] and rotational (0.08−0.10 eV)[117,120,122,123] energies of desorbed CO_2 from CO oxidation on Pd surfaces are smaller than its vibrational energy of antisymmetric mode. Therefore, CO_2 dissociation can be selectively enhanced by exciting the CO_2 stretching vibrational modes.

Finally, I discuss the temperature dependence of the translational energy of CO_2. Experimentally, it was reported that the E_t of desorbed CO_2 from formate decomposition is independent of the surface temperature,[108] while that from CO oxidation is linearly dependent on the surface temperature.[121] From present theoretical simulations, it turns out that at most 20% of E_a(syn) is transferred into surface modes. On the other hand, it can be deduced that approximately 60% of the activation energy of CO_2 dissociation (1.30 eV)[124] on a Pd surface, which is reverse reaction of CO oxidation, is transferred to the surface mode. Both results, namely, the surface temperature dependence and the energy transfer to the surface mode, indicate the strength of the coupling between CO_2 and the surfaces at the TS of reactions. In the case of formate decomposition, CO_2 is weakly bonded as seen in the left panel of Fig. 4.3b. This is in contrast to the case of CO oxidation, where CO_2 was found to spend a significant residence time in the chemisorption well before it desorbs.[125] Moreover, one of the two C−O bond lengths of CO_2 is significantly elongated at the TS of CO oxidation, and carbon and oxygen are strongly bonded to the surface.[126]

4.6 Summaries

In summary, the minimum energy path of CO_2 hydrogenation into formate and the dynamics of formate decomposition into gas phase CO_2 and adsorbed hydrogen have been investigated using density functional theory calculations. Based on the dynamics analysis of formate decomposition, the bending energy of desorbed CO_2 is twice larger than the translational energy. Since formate synthesis from CO_2 and H_2, the reverse reaction of the formate decomposition, is experimentally suggested to occur by the ER type mechanism, present results indicate that the reaction rate of formate synthesis can be enhanced if the bending vibrational mode of CO_2 is excited rather than the translational and/or stretching modes. Meanwhile, these results are quite different from the case of CO_2 dissociation, in which the antisymmetric stretching mode is the key to increasing the dissociation rate. Accordingly, I anticipate that this work may contribute to the future development in controlling the particular molecular vibrational mode for improving catalytic reaction.

This page is intentionally left blank.

Chapter 5

Summary and Future Works

5.1 Summary

In this dissertation, I have studied the CO_2 adsorption and reaction on the Cu surfaces by means of density functional theory. The aim of this dissertation is to understand the following objectives:

1. Dissociative adsorption of CO_2 on the Cu surfaces at low temperature.
2. CO_2 adsortion on the Cu surfaces.
3. The dynamics of CO_2 desorption as a product formate decomposition.

First objective. The detailed mechanism single CO_2 dissociation on the flat, stepped, and kinked Cu surfaces are discussed in Chapter 2. The summaries of this topic are as follow:

1. CO_2 is physisorbed on the flat, stepped, and kinked Cu surfaces with 180° of O−C−O bond angle.
2. The deformation of CO_2 bond angle gives significant effect to the barrier height.
3. The barrier energy of CO_2 dissociation never dropped below 0.60 eV. Thus, CO_2 does not dissociate on the "ideally" flat, stepped or kinked Cu surfaces at low temperature.
4. The CO_2 dissociation on Cu surfaces below 150 K is attributed to other factors such as Cu adatoms, gas phase or condensed CO_2, or other gas phase molecules.
5. CO_2 dissociation may be followed by the Cu−O−Cu chain formation.

Second objective. The thorough study of CO_2 adsorption on the Cu surfaces by means of DFT as well as TPD and XPS studies are discussed in the Chapter 3. Here, I compared the results obtained using the PBE, PBE-D2, and vdW-DF functionals. The summaries of this topic are as follow:

1. The considered functionals give different behaviors in describing CO_2 adsorption potential on Cu surfaces.
2. The PBE produces an almost repulsive potential energy curve for CO_2 adsorption on the flat Cu surface, whereas PBE-D2 and vdW-DFs give deeper potential energy curves.
3. The calculated CO_2 adsorption energies using optB86b-vdW functional on the Cu(111), Cu(221) and Cu(965) surfaces are in the range of $20 - 27$ kJ/mol.
4. The calculated CO_2 adsorption energy on Cu(111) is still underestimated by $3 - 5$ kJ/mol compared with the measured value of 24 kJ/mol at very low coverage.
5. The discrepancy may be due to the aggregation of CO_2 at low coverage, which can lead to stabilization of adsorbed molecules through attractive intermolecular interaction.

Third objective. *Ab initio* molecular dynamics has been performed to elucidate the energy state of translation, vibration, and rotation of desorbed CO_2 from formate decomposition. Here, I compared the results obtained using the PBE, PBE-D2, and vdW-DF functionals. The summaries of my description in the Chapter 4 are as follow:

1. PBE predicts constant translational energy at 0.30 eV after the CO_2 molecule experiences Pauli repulsion in the first 0.1 ps of simulation time. This profile is proportional to the potential energy curve of CO_2 adsorption on Cu(111) surface (mentioned in the Chapter 3).
2. The time evolution profile of CO_2 translational energy calculated using PBE-D2 and vdW-DFs are also proportional to the potential energy curve of CO_2 adsorption on Cu(111) surface. The calculated translational energy using these functionals are in reasonable agreement with the experimental estimation (0.10 eV).
3. The angular distribution of desorbed CO_2 shows quite sharp collimation along the surface normal direction and is in good agreement with experimental results.
4. The calculated rotational energy of desorbed CO_2 varies between $0.08 - 0.11$ eV.
5. The calculated bending mode energy is close to the third excitation of zero-point energy of isolated CO_2 (0.25 ± 0.02 eV).
6. The calculated vibrational energy of the CO_2 symmetric mode varies between $0.05 - 0.11$ eV.

7. The vibrational energy of the antisymmetric mode (1.5 meV) is much smaller than the zero-point energy of isolated CO_2.
8. The bending energy of desorbed CO_2 is twice larger than the translational energy. Since formate synthesis from CO_2 and H_2, the reverse reaction of the formate decomposition,is experimentally suggested to occur by the ER type mechanism, present results indicate that the reaction rate of formate synthesis can be enhanced if the bending vibrational mode of CO_2 is excited rather than the translational and/or stretching modes.
9. The above results are quite different from the case of CO_2 dissociation, in which the antisymmetric stretching mode is the key to increasing the dissociation rate.

I anticipate that the outlook for the future of the discussed topics is quite positive. These studies may give new insight that single CO_2 molecule does not dissociate on ideal clean Cu surfaces. There must be other factors that promote dissociation process. I have shown that the van der Waals interaction is necessary to describe such weakly bound system, *e.g.*, CO_2 adsorption on Cu surface. Moreover, the key point to enhance formate sythesis, which is notably occured in Eley-Rideal mechanism, has been revealed.

5.2 Future plans

The author is aware that the present study is still far from perfect. Thus, some future works are necessary to improve the results and open new insight of related issues.

CO_2 dissociation. In this issue, I am going to consider the effect of another gas phase. Water molecule seems to play important role in the dissociation process. This hypothesis is based on the reports from my collaborator: OH is also one of abundant residual species in addition to CO species that was observed during the spectroscopy measurements. Therefore, the existence of small amount of water molecule may enhance the dissociation of CO_2.

CO_2 desorption form formate decomposition. In this case, I am considering to compare the present results with the dynamics of CO_2 dissociation case. As mentioned in some previous experimental works, the energy state of desorbed CO_2 as a product od CO oxidation, reverse reaction of CO_2 dissociation, depends on the surface temperature. Therefore, it would be another challenge in the point of view of *ab initio* study to clarify this issue.

This page is intentionally left blank.

APPENDIX

A Surface Reactivity

Chemical reactions occur at surfaces between solid surface and liquids or gases. Surfaces are of particular interest not only because they are boundaries where phases meet and because they give us a place to put catalysts. The surface of solid is intrinsically different from the rest of solid bulk. The bonding at the surface is different with the bulk. Therefore, the chemistry of the surface should be unique. There are two general factors that determine the surface reactivity, electronic affect and geometrical effect.[127]

A.1 Electronic effects in surface reactivity

The argument of the *d* band model are quite general to understand the interactions between adsorbate and metal surface in the transition state as well as in the initial and final states of the reaction. Particularly, the chemical bond formation encompasses the uniqueness of localized *d*-electron in transition metal. Figure 1 shows an illustration of the resulting electron density of states projected onto the adsorbate in Newns-Anderson model for two different cases.[128,129] In this model, the hopping matrix element is often used to denote the interaction strength between the adsorbate wave function of specific electronic level and the metal states. When the band width of the metal states of interest is much bigger than the hopping matrix element, the interaction leads to a broadened resonance-level of the projected states on the adsorbate (upper part of Fig. 1). The bottom of the resonance would reflect more bonding and the upper part more anti-bonding character. Meanwhile, the bonding and anti-bonding states separate out as new distinct electronic levels, below and above free adsorbate level, if the metal band width is much smaller than the hopping matrix. The latter is usually the case upon interaction with more localized *d*-states and the former for the delocalized *s*- and *p*-states.

Those two cases can be directly observed by using X-ray spectroscopy and/or by ultraviolet photo-electron. In the case of nitrogen on Cu(100),[130] the *p*-states of nitrogen atom are split into two distinct levels which are bonding and antibonding, respectively. This represents the case when the width of metal *d*-band is narrower than the hopping matrix. In the meantime, the opposite case, i.e., when band width is much broader

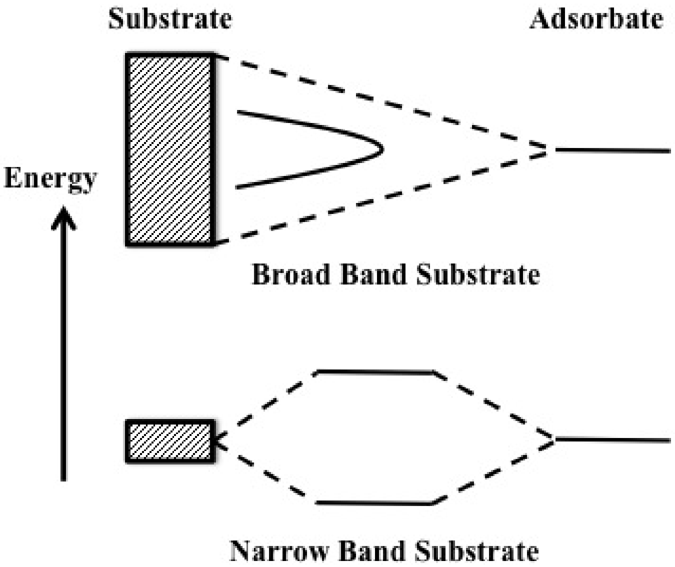

Figure 1: Projected adsorbate density of states in the Newns-Aderson model in two limiting case: top) when the band width is larger and bottom) when the band width is smaller than the hopping matrix element.

than the hopping matrix, was observed in adsorbed Ar on Ag(110) by using XAS.[131] Since Ar using the Z + 1 approximation becomes K as an effect of the final core hole state, we could see that the K 4*s* level becomes a broad asymmetric resonance. The adsorbate resonance has a tail towards lower energies with clear cut-off at the Fermi level. This indicates that the 4*s* level interacts with the delocalized unoccupied Ag *sp* electrons. Thus, the charge transfer takes place from adsorbate to the substrate.

In case of dissociative adsorption, when the covalent bond of adsorbate cleaves, the unpaired electrons will exist to make a bond with unsaturated states of surface metal atoms. This bonding mechanism is denoted as radical adsorption. The simple picture of the electronic structure when an atomic adsorbate interacts with a transition metal is usually denoted as d-band model.

Figure 2, reproduced from Nilsson *et al.*,[132] shows the illustration of adsorbate valence state interacting with the metal states on the transition metal. The valence state of the transition metal can be divided into the free-electron-like *s*-electron states and localized *d*-electron states. The interaction with *s*-electron would lead to a broad resonance whereas interaction with *d*-electron would lead to distinct new levels. The coupling to the broad *s*-band then leads to a broadening and shift of the adsorbate state (Fig. 2).[129,132] Since all the transition metals have a half-filled *s*-band in the metallic state and since the band is broad, there will be only small differences in this interaction from one metal to the next ones.

The differences among the transition metals should be associated primarily with the *d*-states. The interaction of adsorbate with the *d*-states will lead to the bonding and

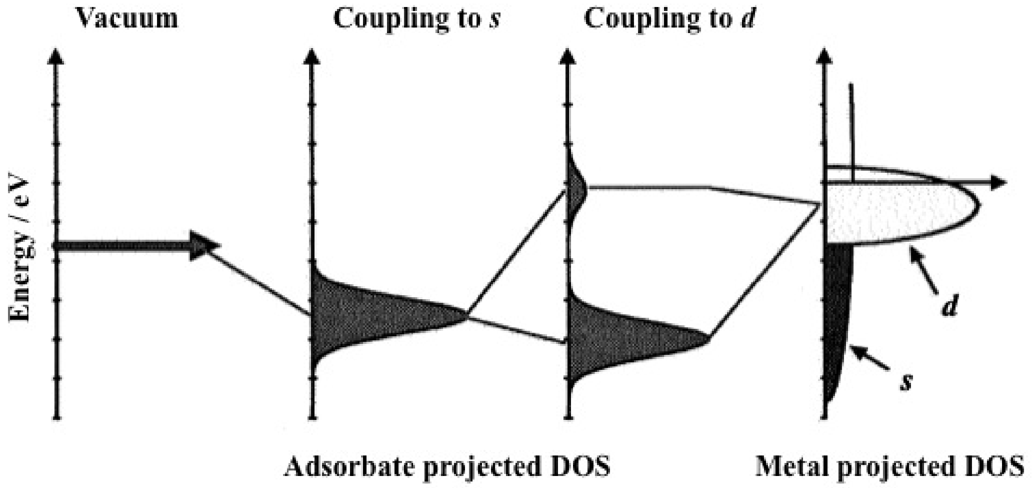

Figure 2: Illustration of the formation of a chemical bond between an adsorbate valance level and the *s*- and *d*-states of metal surface.

anti-bonding states. When these two states are formed, the bond strength will depend on the relative occupancy of these states. If the bonding states are fully occupied, there will be a strong bond. While, the bond becomes considerably weaker if the anti-bonding states are also filled. The number of anti-bonding states that are above the Fermi level depends on the metal itself. As the *d*-states shift up in energy from the late transition metal (Cu) towards the left in the early transition-metal, the strength of the adsorbate-metal bond should increase.

A.2 Geometrical effects in surface reactivity

The geometrical effect in heterogeneous catalysis was first introduced by Taylor in 1925.[133] At present, theoretical studies have helped giving ideas about the effects itself and experimentally it has been shown to be correct. An additional geometrical effect of surface on the reactivity of transition metal surfaces was reported previously in N_2 activation[134] and NO dissociation[135] on Ru(0001) surface. The stepped Ru surface has lower barrier for N_2 and NO dissociation than the close-packed (0001) surface. One of the reason is because the Ru step atoms have higher-lying d states and thus the transition states stabilize.

The effect of geometrical changes was reported comprehensively by Hammer in the case of NO dissociation.[136] By introducing some steps, the Ru surface reactivity was changed. On the terrace region, N and O atom shared two Ru atoms at the same time in the transition state. Meanwhile, sharing two metal atom could be avoided near the step edge. It was reported that sharing nearest-neighbor metal atoms enhances the repulsive force between the reaction products and thus destabilizes the transition state. The prohibition of sharing two metal atoms also reported by Michaelides *et al.*.[137]

The study of geometrical effect was also reported before in the CO dissociation on flat, stepped, and kinked Pd and Rh surfaces.[138] It was reported that the stability of transition states were described from bonding competition effect and direct Pauli repulsion in term of interaction energy (E_{int}). The presence of step or kink sites is important in reducing the barrier.

B Brønsted-Evans-Polanyi Relationship in Heterogeneous Catalysis

Many industrial scale production of chemicals proceeds with the aid of a solid catalyst and consists of elementary reactions at catalytic surfaces. The activation energy controls the rate of each elementary reaction step in catalytic cycles. There is such linear correlation between activation energies and reaction energies. The concept was introduced firstly by Brønsted[139] and Evans and Polanyi.[140] Nowadays, it becomes more convenient to study the relation between activation energies and reaction energies in such Brønsted-Evans-Polanyi (BEP) relationship since DFT calculations were introduced.

The BEP relationship is believed to be applicable to many reactions in heterogeneous catalysts. Some considerable evidences have performed from theoretical studies for specific reaction system.[137,141,142] In principle, the specific reaction on considered metal surface and its geometry has different BEP lines. For example, the N_2 dissociation reactions on stepped metal surfaces have lower activation energies than those on flat metal surfaces.[143]

We may question why there is linear relationship between E_{a} and ΔE, and why the BEP relationship is structure dependent and adsorbate-independent. The nature of transition structure can provide answers to those questions. For a given metal surface geometry, the transition state is essentially independent of some molecule and the metal considered. The bond length or bond angle in the transition state is quite different with those in the initial state, and the adsorbates have largely lost their molecular identity. This means that the variations in the transition state energy will follow that of the final state energy closely giving a linear relationship with slope close to one. The transition state depends on its local surface structure, therefore the BEP lines are different for flat and defected surfaces. Since the surface geometries at transition states are so similar among different adsorbates, then the BEP relationship is adsorbate-independent. The universal relationship between activation energy and binding energy suggest a general approach to find new catalyst materials with the best characteristic, which have low activation energy and weak bonding of intermediates.[141]

There are three classes of BEP line for elementary dissociation reactions at surfaces that have been reported previously.[137] The first class is dehydrogenation reactions, for example O−H cleavage in H_2O or C−H cleavage in CH_x fragments. The BEP relationship of this class is identified as (in eV):

$$E_{\mathrm{a}}^{\mathrm{diss}} = (0.92 \pm 0.05)\Delta H + 0.87 \pm 0.05 \tag{1}$$

where ΔH is enthalpy changes. The second class is diatomic activation and hydrocarbon cracking. This class involves dissociation of stable diatomic molecules such as N_2 or O_2, and C−C bond cleavage in C_2H_4. The BEP relationship of this class is identified as (in eV):

$$E_{\mathrm{a}}^{\mathrm{diss}} = (0.97 \pm 0.05)\Delta H + 1.69 \pm 0.15 \tag{2}$$

The last class is triatomic activation which comprises CO_2 and also similar doubly bonded molecules such as NO_2 and N_2O. In this class, the dependence on ΔH relative to first and second classes has been reduced:

$$E_{\mathrm{a}}^{\mathrm{diss}} = (0.74 \pm 0.05)\Delta H + 1.03 \pm 0.08 \tag{3}$$

By referring to those three classes, it may be possible to estimate the activation energy for a chemical reaction in heterogeneous catalyst merely from information on adsorption energies.

C AIMD trajectories

The additional samples of initial geometry for AIMD simulations had been considered. The additional geometries were derived from the original TS geometry (shown in Fig. 3 and Table 1) by slightly moving the atoms within a hyperplane perpendicular to the reaction coordinate. In this procedure, we moved the atoms towards the second, third, fourth, fifth, and sixth lowest normal mode vectors from the TS, which were obtained from the vibrational frequency analysis. The displacement was done so that the new initial geometry has 0.02 eV energy different with the original initial geometry. The additional calculations were done using optB86b-vdW functional. As shown in the Table 2, the average calculation results from several samples of AIMD trajectory indicate that most of formate synthesis energy is transferred into bending mode of CO_2.

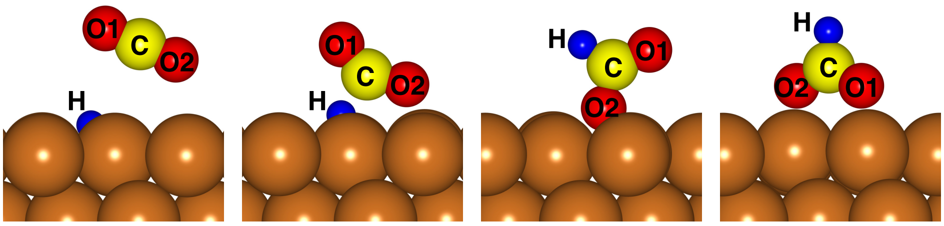

Figure 3: From left to right panel: configuration of Initial state (IS), transition state (TS), monodentate formate (mo-HCOO), and bidentate formate (bi-HCOO) structures, respectively. The red, yellow, blue, and brown circles represent oxygen, carbon, hydrogen, and Cu atoms, respectively.

Table 1: Detailed descriptions of the structures depicted in Fig. S3. The bond length (C−O1, C−O2, and C−H) and bond distance (Cu−O2 and Cu−H), and bond angle are in Å and degree, respectively.

	PBE	PBE-D2	vdW-DF1	rev-vdW-DF2	optB86b-vdW
Initial state					
C−O1	1.18	1.18	1.18	1.18	1.18
C−O2	1.18	1.18	1.18	1.18	1.18
C−H	2.97	2.98	3.12	2.90	2.91
Cu−O2	3.30	2.98	3.21	2.90	2.92
Cu−H	0.88	0.87	0.85	0.89	0.88
$\angle_{\text{O1−C−O2}}$	179.81	179.60	179.93	179.84	179.82
Transition state					
C−O1	1.20	1.20	1.20	1.20	1.20
C−O2	1.23	1.24	1.24	1.25	1.24
C−H	1.58	1.49	1.49	1.51	1.48
Cu−O2	2.17	2.13	2.23	2.06	2.13
Cu−H	1.35	1.31	1.25	1.31	1.20
$\angle_{\text{O1−C−O2}}$	147.04	144.27	144.83	143.36	144.59
Monodentate formate					
C−O1	1.22	1.22	1.22	1.22	1.22
C−O2	1.35	1.35	1.36	1.36	1.36
C−H	1.11	1.11	1.11	1.11	1.11
Cu−O2	1.40	1.39	1.41	1.40	1.40
Cu−H	3.35	3.34	3.36	3.36	3.34
$\angle_{\text{O1−C−O2}}$	124.27	124.07	124.13	123.92	123.92
Bidentate formate					
C−O1	1.27	1.27	1.28	1.27	1.27
C−O2	1.27	1.27	1.28	1.27	1.27
C−H	1.11	1.11	1.10	1.11	1.11
Cu−O2	2.02	2.01	2.05	2.01	2.01
Cu−H	3.67	3.68	3.75	3.73	3.75
$\angle_{\text{O1−C−O2}}$	127.82	127.56	127.63	127.46	127.49

Table 2: Calculated translational energy (E_{t}), rotational energy (E_{r}), vibrational energy of bending mode (E_{b}), and vibrational energy of symmetric stretching mode (E_{s}) of desorbed CO_2 from formate decomposition on Cu(111) calculated using optB86b-vdW functional (in eV). The AIMD simulations were done starting from different initial geometries that were derived from the original TS geometries by slightly moving the atoms within a hyperplane perpendicular to the reaction coordinate

	First	Second	Third	Fourth	Fifth	Sixth	Average
E_{t}	0.11	0.14	0.16	0.12	0.18	0.11	0.14[a]
E_{r}	0.10	0.09	0.11	0.09	0.17	0.07	0.11
E_{b}	0.25	0.27	0.24	0.26	0.22	0.30	0.26
E_{s}	0.07	0.02	0.03	0.05	0.01	0.03	0.04
Surf. mode[b]	0.02	0.03	0.01	0.03	0.07	0.04	0.03

[a] The calculated CO_2 translational energy as a formate decomposition product is in good agreement with experimentally reported results in Ref. 108.

[b] This energy is deduced from the following: $E_{\mathrm{a}}(\mathrm{syn}) - (E_{\mathrm{t}} + E_{\mathrm{r}} + E_{\mathrm{b}} + E_{\mathrm{s}})$.

BIBLIOGRAPHY

[1] K. Weissermel and H.-J. Arpe, “Industrielle organische chemie,” (Verlag Chemie, Weinheim, 1976).

[2] U. Burghaus, Prog. Surf. Sci. **89**, 161 (2014).

[3] D. W. Stephan, Nature **459**, 54 (2013).

[4] G. A. Olah, A. Goeppert, and G. K. S. Prakash, J. Org. Chem. **74**, 487 (2009).

[5] H.-J. Freund and M. Roberts, Surf. Sci. Rep. **25**, 225 (1996).

[6] C.-S. Chen, W.-H. Cheng, and S.-S. Lin, Catal. Lett. **68**, 45 (2000).

[7] G. Chinchen, P. Denny, D. Parker, M. Spencer, and D. Whan, Appl. Catal. **30**, 333 (1987).

[8] S. Kattel, P. J. Ramírez, J. G. Chen, J. A. Rodriguez, and P. Liu, Science **355**, 1296 (2017).

[9] S. Kuld, M. Thorhauge, H. Falsig, C. F. Elkjær, S. Helveg, I. Chorkendorff, and J. Sehested, Science **352**, 969 (2016).

[10] M. Behrens, F. Studt, I. Kasatkin, S. Kühl, M. Hävecker, F. Abild-Pedersen, S. Zander, F. Girgsdies, P. Kurr, B.-L. Kniep, M. Tovar, R. W. Fischer, J. K. Nørskov, and R. Schlögl, Science **336**, 893 (2012).

[11] L. C. Grabow and M. Mavrikakis, ACS Catal. **1**, 365 (2011).

[12] T. Fujitani, I. Nakamura, T. Uchijima, and J. Nakamura, Surf. Sci. **383**, 285 (1997).

[13] G. Wang, Y. Morikawa, T. Matsumoto, and J. Nakamura, J. Phys. Chem. B **110**, 9 (2006).

[14] H. Nakano, I. Nakamura, T. Fujitani, and J. Nakamura, J. Phys. Chem. B **105**, 1355 (2001).

[15] H. Nishimura, T. Yatsu, T. Fujitani, T. Uchijima, and J. Nakamura, J. Mol. Catal. A-Chem. **155**, 3 (2000).

[16] I. Nakamura, H. Nakano, T. Fujitani, T. Uchijima, and J. Nakamura, J. Vac. Sci. Technol. A **17**, 1592 (1999).

[17] C. Song, Catal. Today **115**, 2 (2006).

[18] G. C. Chinchen, P. J. Denny, D. G. Parker, M. S. Spencer, and D. A. Whan, Appl. Catal **30**, 333 (1986).

[19] M. Behrens, F. Studt, I. Kasatkin, S. Kühl, M. Hävecker, F. Abild-Pedersen, S. Zander, F. Girgsdies, P. Kurr, B.-L. Kniep, M. Tovar, R. W. Fischer, J. K. Nørskov, and R. Schlögl, Science **336**, 893 (2012).

[20] C.-S. Chen, W.-H. Cheng, and S.-S. Lin, Catal. Lett. **68**, 45 (2000).

[21] J. Nakamura, J. A. Rodriguez, and C. T. Campbell, J. Phys.: Condens. Matter **1**, SB149 (1989).

[22] P. B. Rasmussen, P. A. Taylor, and I. Chorkendorff, Surf. Sci. **269**, 352 (1992).

[23] K.-H. Ernst, D. Schlatterbeck, and K. Christmann, Phys. Chem. Chem. Phys. **1**, 4105 (1999).

[24] S. S. Fu and G. A. Somorjai, Surf. Sci. **262**, 68 (1992).

[25] I. A. Bönicke, W. Kirstein, and F. Thieme, Surf. Sci. **307**, 177 (1994).

[26] T. Koitaya, Y. Shiozawa, K. Mukai, S. Yoshimoto, and J. Yoshinobu, "14th International Conference on Vibrations at Surfaces in Kobe (Japan)," (2012), and personal communication.

[27] D. B. Cao, Y. W. Li, J. Wang, and H. Jiao, Surf. Sci. **603**, 2991 (2009).

[28] H. Wu, N. Zhang, H. Wang, and S. Hong, Chem. Phys. Lett. **568**, 84 (2013).

[29] A. A. Gokhale, J. A. Dumesic, and M. Mavrikakis, J. Am. Chem. Soc. **130**, 1402 (2008).

[30] T. Jiang, D. J. Mowbray, S. Dobrin, H. Falsig, B. Hvolbæk, B. T. Bligaard, and J. K. Nørskov, J. Phys. Chem. C **113**, 10548 (2009).

[31] S. Liu, P. Jin, C. Hao, D. Zhang, X. Yang, and S. Chen, Appl. Surf. Sci. **258**, 3980 (2012).

[32] Y. Morikawa, K. Iwata, J. Nakamura, T. Fujitani, and K. Terakura, Chem. Phys. Lett. **304**, 91 (1999).

[33] Y. Morikawa, K. Iwata, and K. Terakura, Appl. Surf. Sci. **169**, 11 (2001).

[34] R. W. G. Wyckoff, "Crystals structures," (Wiley, New York, 1963).

[35] G. Mills, H. Jónsson, and G. K. Schenter, Surf. Sci. **324**, 305 (1995).

[36] G. Henkelman, B. P. Uberuaga, and H. Jónsson, J. Chem. Phys. **113**, 9901 (2000).

[37] J. P. Perdew, K. Burke, and M. Ernzerhof, Phys. Rev. Lett. **77**, 3865 (1996).

[38] D. Vanderbilt, Phys. Rev. B **77**, R7892 (1990).

[39] S. Grimme, J. Comput. Chem. **27**, 1787 (2006).

[40] G. Wang, Y. Morikawa, T. Matsumoto, and J. Nakamura, J. Phys. Chem. B **110**, 9 (2006).

[41] E. B. Wilson, J. C. Decius, and P. C. Cross, "Molecular vibrations," (Dover Publications, Inc., New York, 1955) Chap. 4.

[42] M. Dion, H. Rydberg, E. Schröder, D. C. Langreth, and B. I. Lundqvist, Phys. Rev. Lett. **92**, 246401 (2004).

[43] M. Dion, H. Rydberg, E. Schröder, D. C. Langreth, and B. I. Lundqvist, Phys. Rev. Lett. **95**, 109902 (2005).

[44] P. Lazić, M. Alaei, N. Atodiresei, V. Caciuc, R. Brako, and S. Blügel, Phys. Rev. B **81**, 045401 (2010).

[45] Y. Zhang and W. Yang, Phys. Rev. Lett. **80**, 890 (1998).

[46] K. Johnston, J. Kleis, B. I. Lundqvist, and R. M. Nieminen, Phys. Rev. B **77**, 121404 (2008).

[47] I. Hamada, K. Lee, and Y. Morikawa, Phys. Rev. B **81**, 115452 (2010).

[48] J. Braun, A. P. Graham, F. Hofmann, W. Silvestri, J. P. Toennies, and G. Witte, J. Chem. Phys. **105**, 3258 (1996).

[49] S. Vollmer, G. Witte, and C. Wöll, Catal. Lett. **77**, 97 (2001).

[50] M. Gajdoš, A. Eichler, J. Hafner, G. Meyer, and K.-H. Rieder, Phys. Rev. B **71**, 035402 (2005).

[51] F. Mehmood, A. Kara, T. S. Rahman, and K. P. Bohnen, Phys. Rev. B **74**, 155439 (2006).

[52] P. Hollins and J. Pritchard, Surf. Sci. **89**, 486 (1979).

[53] R. Ryberg, Surf. Sci. **114**, 627 (1982).

[54] J. Radnik and H.-J. Ernst, J. Chem. Phys. **110**, 10522 (1999).

[55] G. Glockler, J. Phys. Chem. **62**, 1049 (1958).

[56] D. F. Eggers and B. L. Crawford, J. Chem. Phys. **19**, 1554 (1951).

[57] H.-J. Freund and M. W. Roberts, Surf. Sci. Rep. **25**, 225 (1996).

[58] M. Giesen-Seibert, R. Jentjens, M. Poensgen, and H. Ibach, Phys. Rev. Lett. **71**, 3521 (1993).

[59] S. Horch, H. T. Lorensen, S. Helveg, E. Lægsgaard, I. Stengsgaard, K. W. Jacobsen, J. K. Nørskov, and F. Besenbacher, Nature **398**, 134 (1998).

[60] T. Koitaya, Y. Shiozawa, K. Mukai, S. Yoshimoto, and J. Yoshinobu, J. Chem. Phys. **144**, 054703 (2016).

[61] T. Koitaya, S. Yamamoto, Y. Shiozawa, K. Takeuchi, R.-Y. Liu, K. Mukai, S. Yoshimoto, K. Akikubo, I. Matsuda, and J. Yoshinobu, Top. Catal. **59**, 526 (2016).

[62] F. Muttaqien, Y. Hamamoto, K. Inagaki, and Y. Morikawa, J. Chem. Phys. **141**, 034702 (2014).

[63] B. Eren, R. S. Weatherup, N. Liakakos, G. A. Somorjai, and M. Salmeron, J. Am. Chem. Soc. **138**, 8207 (2016).

[64] I. A. Bönicke, W. Kirstein, and F. Thieme, Surf. Sci. **307**, 177 (1994).

[65] P. Rasmussen, P. Holmblad, H. Christoffersen, P. Taylor, and I. Chorkendorff, Surf. Sci. **287**, 79 (1993).

[66] R. G. Copperthwaite, P. R. Davies, M. A. Morris, M. W. Roberts, and R. A. Ryder, Catal. Lett. **1**, 11 (1988).

[67] G.-C. Wang, L. Jiang, Y. Morikawa, J. Nakamura, Z.-S. Cai, Y.-M. Pan, and X.-Z. Zhao, Surf. Sci. **570**, 205 (2004).

[68] Y.-F. Zhao, Y. Yang, C. Mims, C. H. Peden, J. Li, and D. Mei, J. Catal. **281**, 199 (2011).

[69] Y. Morikawa, K. Iwata, J. Nakamura, T. Fujitani, and K. Terakura, Chem. Phys. Lett. **304**, 91 (1999).

[70] S. D. Chakarova-Käck, E. Schröder, B. I. Lundqvist, and D. C. Langreth, Phys. Rev. Lett. **96**, 146107 (2006).

[71] K. Toyoda, Y. Nakano, I. Hamada, K. Lee, S. Yanagisawa, and Y. Morikawa, Surf. Sci. **603**, 2912 (2009).

[72] K. Toyoda, Y. Nakano, I. Hamada, K. Lee, S. Yanagisawa, and Y. Morikawa, J. Electron Spectros. Relat. Phenom. **174**, 78 (2009), advanced Spectroscopies of Molecular Materials for Electronics.

[73] P. J. Feibelman, B. Hammer, J. K. Norskov, F. Wagner, M. Scheffler, R. Stumpf, R. Watwe, and J. Dumesic, J. Phys. Chem. B **105**, 4018 (2001).

[74] M. Dion, H. Rydberg, E. Schröder, D. C. Langreth, and B. I. Lundqvist, Phys. Rev. Lett. **92**, 246401 (2004).

[75] M. Dion, H. Rydberg, E. Schröder, D. C. Langreth, and B. I. Lundqvist, Phys. Rev. Lett. **95**, 109902 (2005).

[76] K. Berland, V. R. Cooper, K. Lee, E. Schröder, T. Thonhauser, P. Hyldgaard, and B. I. Lundqvist, Rep. Prog. Phys. **78**, 066501 (2015).

[77] K. Lee, E. D. Murray, L. Kong, B. I. Lundqvist, and D. C. Langreth, Phys. Rev. B **82**, 081101 (2010).

[78] V. R. Cooper, Phys. Rev. B **81**, 161104 (2010).

[79] O. A. Vydrov and T. Van Voorhis, J. Chem. Phys. **133**, 244103 (2010).

[80] J. Klimeš, D. R. Bowler, and A. Michaelides, Phys. Rev. B **83**, 195131 (2011).

[81] J. Wellendorff, K. T. Lundgaard, A. Møgelhøj, V. Petzold, D. D. Landis, J. K. Nørskov, T. Bligaard, and K. W. Jacobsen, Phys. Rev. B **85**, 235149 (2012).

[82] R. Sabatini, T. Gorni, and S. de Gironcoli, Phys. Rev. B **87**, 041108 (2013).

[83] I. Hamada, Phys. Rev. B **89**, 121103 (2014).

[84] K. Berland and P. Hyldgaard, Phys. Rev. B **89**, 035412 (2014).

[85] K. Takeuchi, S. Yamamoto, Y. Hamamoto, Y. Shiozawa, K. Tashima, H. Fukidome, T. Koitaya, K. Mukai, S. Yoshimoto, M. Suemitsu, Y. Morikawa, J. Yoshinobu, and I. Matsuda, J. Phys. Chem. C **121**, 2807 (2017).

[86] B. Vlaisavljevich, J. Huck, Z. Hulvey, K. Lee, J. A. Mason, J. B. Neaton, J. R. Long, C. M. Brown, D. Alfé, A. Michaelides, and B. Smit, J. Phys. Chem. A **121**, 4139 (2017).

[87] K. Czelej, K. Cwieka, and K. J. Kurzydlowski, Catal.Comm. **80**, 33 (2016).

[88] K. Lee, J. D. Howe, L.-C. Lin, B. Smit, and J. B. Neaton, Chem. Mater. **27**, 668 (2015).

[89] L. Dietz, S. Piccinin, and M. Maestri, The Journal of Physical Chemistry C **119**, 4959 (2015).

[90] F. Studt, F. Abild-Pedersen, J. B. Varley, and J. K. Nørskov, Catal. Lett. **143**, 71 (2013).

[91] S. Grimme, J. Comput. Chem. **27**, 1787 (2006).

[92] Y. Morikawa, K. Iwata, and K. Terakura, Appl. Surf. Sci. **169-170**, 11 (2001).

[93] Y. Hamamoto, I. Hamada, K. Inagaki, and Y. Morikawa, Phys. Rev. B **93**, 245440 (2016).

[94] B. Lang, R. Joyner, and G. Somorjai, Surf. Sci. **30**, 44 (1972).

[95] J. Wu and F. Gygi, J. Chem. Phys. **136**, 224107 (2012).

[96] G. Román-Pérez and J. M. Soler, Phys. Rev. Lett. **103**, 096102 (2009).

[97] D. Vanderbilt, Phys. Rev. B **41**, 7892 (1990).

[98] T. Koitaya, Y. Shiozawa, Y. Yoshikura, K. Mukai, S. Yoshimoto, S. Torii, F. Muttaqien, Y. Hamamoto, K. Inagaki, Y. Morikawa, and J. Yoshinobu, Surf. Sci. **663**, 1 (2017).

[99] L. Baker, B. Holsclaw, A. E. Baber, H. L. Tierney, E. C. H. Sykes, and A. J. Gellman, J. Phys. Chem. C **114**, 18566 (2010).

[100] H. Schlichting and D. Menzel, Rev. Sci. Instrum. **64**, 2013 (1993).

[101] P. Feulner and D. Menzel, J. Vac. Sci. Technol. **17**, 662 (1980).

[102] R. Raval, S. Parker, and M. Chesters, Surf. Sci. **289**, 227 (1993).

[103] D. R. Lide, "CRC Handbook of Chemistry Physics," (CRC Press, Boca Raton, Ohio, 1998).

[104] J. B. Miller, H. R. Siddiqui, S. M. Gates, J. N. Russell Jr., J. T. Yates Jr., J. C. Tully, and M. J. Cardillo, J. Chem. Phys. **87**, 6725 (1987).

[105] E. Habenschaden and J. Küppers, Surface Science **138**, L147 (1984).

[106] T. Shimanouchi, *Tables of Molecular Vibrational Frequencies, Consolidated Volume 1* (National Standard Reference Data System (NSRDS), Tokyo, Japan, 1972).

[107] R. A. Hadden, H. D. Vandervell, K. C. Waugh, and G. Webb, in *Proc. 9th Int. Cong. on Catalysis*, Vol. 4, edited by M. J. Philips and M. Ternan (The Chemical Institute of Canada, Ottawa, 1988) p. 1835.

[108] J. Quan, T. Kondo, G. Wang, and J. Nakamura, Angew. Chem. Int. Edit. **56**, 3496 (2017).

[109] J. A. Herron, Y. Morikawa, and M. Mavrikakis, P. Natl. Acad. Sci. USA **113**, E4937 (2016).

[110] T. Thonhauser, V. R. Cooper, S. Li, A. Puzder, P. Hyldgaard, and D. C. Langreth, Phys. Rev. B **76**, 125112 (2007).

[111] G. Mills, H. Jónsson, and G. K. Schenter, Surf. Sci. **324**, 305 (1995).

[112] G. Henkelman, B. P. Uberuaga, and H. Jónsson, J. Chem. Phys. **113**, 9901 (2000).

[113] W. B. Person and G. Zerbi, *Vibrational intensities in infrared and Raman spectroscopy* (Elsevier Scientific Pub. Co., Amsterdam, Netherland, 1982).

[114] G. Herzberg, *Electronic Spectra and Electronic Structure of Polyatomic Molecules* (D. Van Nostrand Co., Inc., Princeton, New Jersey, 1966).

[115] B. Jiang and H. Guo, J. Chem. Phys. **138**, 234104 (2013).

[116] B. Jiang and H. Guo, J. Chem. Phys. **144**, 091101 (2016).

[117] T. Yamanaka, Phys. Chem. Chem. Phys. **10**, 5429 (2008).

[118] K. Nakao, S. Ito, K. Tomishige, and K. Kunimori, Catal. Today **111**, 316 (2006).

[119] K. Nakao, S. Ito, K. Tomishige, and K. Kunimori, Chem. Phys. Lett. **410**, 86 (2005).

[120] K. Nakao, S. Ito, K. Tomishige, and K. Kunimori, J. Phys. Chem. B **109**, 17553 (2005).

[121] K. Kimura, Y. Ohno, and T. Matsushima, Surf. Sci. **429**, L455 (1999).

[122] H. Uetsuka, K. Watanabe, H. Ohnuma, and K. Kunimori, Surf. Sci. **377**, 765 (1997).

[123] H. Uetsuka, K. Watanabe, and K. Kunimori, Surf. Sci. **363**, 73 (1996).

[124] T. Engel and G. Ertl, J. Chem. Phys. **69**, 1267 (1978).

[125] X. Zhou, B. Kolb, X. Luo, H. Guo, and B. Jiang, J. Phys. Chem. C **121**, 5594 (2017).

[126] A. Alavi, P. Hu, T. Deutsch, P. L. Silvestrelli, and J. Hutter, Phys. Rev. Lett. **80**, 3650 (1998).

[127] J. M. Thomas and W.-J. Thomas, "Principle and practice of heterogeneous catalysis," (Wiley-VCH, Wienheim, 1997).

[128] P. W. Anderson, Phys. Rev. **124**, 41 (1961).

[129] D. M. Newns, Phys. Rev. **178**, 1123 (1969).

[130] T. Wiell, J. E. Klepais, P. Bennich, O. Björneholm, N. Wassdahl, and A. Nilsson, Phys. Rev. B **58**, 1655 (1998).

[131] A. Sandell, O. Hjortstam, A. Nilsson, P. A. Brühwiler, O. Eriksson, P. Bennich, P. Rudolf, J. M. Wills, B. Johansson, and N. Mårtensson, Phys. Rev. Lett. **78**, 4994 (1997).

[132] A. Nilsson, L. G. M. Pettersson, B. Hammer, T. Bligaard, C. H. Christensen, and J. K. Nørskov, Catal. Lett. **100**, 111 (2005).

[133] H. S. Taylor, Proc. R. Soc. London Ser. A **108**, 105 (1925).

[134] S. Dahl, A. Logadottir, R. C. Egeberg, J. H. Larsen, I. Chorkendorff, E. Törnqvist, and J. K. Nørskov, Phys. Rev. Lett. **83**, 1814 (1999).

[135] B. Hammer, Phys. Rev. Lett. **83**, 3681 (1999).

[136] B. Hammer, Surf. Sci. **459**, 323 (2000).

[137] A. Michaelides, Z.-P. Liu, C. J. Zhang, A. Alavi, D. A. King, and P. Hu, J. Am. Chem. Soc. **125**, 3704 (2003).

[138] Z.-P. Liu and P. Hu, J. Am. Chem. Soc. **125**, 1958 (2003).

[139] N. Brønsted, Chem. Rev. **5**, 231 (1928).

[140] M. G. Evans and M. Polanyi, Trans. Faraday Soc. **34**, 11 (1938).

[141] J. K. Nørskov, T. Bligaard, A. Logadottir, S. Bahn, L. Hansen, M. Bollinger, H. Bengaard, B. Hammer, Z. Sljivancanin, M. Mavrikakis, Y. Xu, S. Dahl, and C. J. H. Jacobsen, J. Catal. **209**, 275 (2002).

[142] Z.-P. Liu and P. Hu, J. Chem. Phys. **114**, 8244 (2001).

[143] A. Logadottir, T. H. Rod, J. K. Nørskov, B. Hammer, S. Dahl, and C. J. H. Jacobsen, J. Catal. **197**, 229 (2001).

This page is intentionally left blank.

ACKNOWLEDGEMENT

All praises to Allah SWT, the Most Gracious and the Most Merciful, and His Messanger for all the blessing in completing this doctor dissertation. First, I thank my wife and my son who always support me during my study. I am sorry that I sometimes fail to deal with our family time and my study. I also thank my family in Indonesia who always support and bless me.

I thank Morikawa sensei who guides me in this research. I also thank to Hamada sensei, Inagaki sensei, Kizaki sensei, and Hamamoto sensei for giving me such good advices and comments in improving the quality of my knowledge. I thank Prof. Y. Kuwahara, Prof. M. Okada, and Prof. T. Oguchi for being my vice reviewer in the doctoral thesis. I specially thank Prof. J. Yoshinobu and Dr. T. Koitaya for providing their experimental results prior to publication and for the stimulating discussions. I also specially thank Prof. J. Nakamura, Prof. Kondo, and Dr. J. Quan for valuable discussions. The present work was supported by the Advanced Catalytic Transformation Program for Carbon utilization (ACT-C), (Grant No. JPMJCR12YU), of the Japan Science and Technology Agency (JST), and partly supported by Grants-in Aid for Scientific Research on Innovative Areas 3D Active-Site Science (No. 26105010 and No. 26105011) from the Japan Society for the Promotion of Science (JSPS), the Elements Strategy Initiative for Catalysts and Batteries (ESICB) supported by the Ministry of Education, Culture, Sports, Science, and Technology, Japan (MEXT). The numerical calculations were performed in the computer resources at the Institute for Solid State Physics (ISSP), the Univ. of Tokyo and the HPCI systems provided by Nagoya Univ., the Univ. of Tokyo, and Tohoku Univ. through the HPCI System Research Project (Project ID: hp130112, hp140166, and hp150201).

July 2017

Author

This page is intentionally left blank.

BIOGRAPHY

List of publications:

1. **Fahdzi Muttaqien**, Y. Hamamoto, K. Inagaki, and Y. Morikawa, “Dissociative Adsorption of CO_2 on Flat, Stepped, and Kinked Cu Surfaces”, Journal of Chemical Physics, American Institute of Physics, vol. **141**, 034702-1-6 (2014), DOI: 10.1063/1.4887362.

2. **Fahdzi Muttaqien**, H. Oshima, Y. Hamamoto, K. Inagaki, I. Hamada, and Y. Morikawa, “Desorption Dynamics of CO_2 from Formate Decomposition on Cu(111)”, Chemical Communications, The Royal Society of Chemistry, vol. **53**, 9222-9225 (2017), DOI: 10.1039/c7cc03707d.

3. **Fahdzi Muttaqien**, Y. Hamamoto, I. Hamada, K. Inagaki, Y. Shiozawa, K. Mukai, T. Koitaya, S. Yoshimoto, J. Yoshinobu, and Y. Morikawa, “CO_2 Adsorption on the Copper Surfaces: van der Waals Density Functional and TPD Studies”, Accepted for publication in the Journal of Chemical Physics, American Institute of Physics, vol. 147 (2017).

4. T. Koitaya, Y. Shiozawa, Y. Yoshikura, K. Mukai, S. Yoshimoto, S. Torii, **Fahdzi Muttaqien**, Y. Hamamoto, K. Inagaki, Y. Morikawa, and J. Yoshinobu, "Electronic states and growth modes of Zn atoms deposited on Cu(111) studied by XPS, UPS and DFT", Surface Science, Elsevier, vol. **663**, 1-10 (2017), DOI: 10.1016/j.susc.2017.03.015.

List of conferences:

1. **Fahdzi Muttaqien**, Y. Hamamoto, K. Inagaki, and Y. Morikawa, “Dissociative Adsorption of CO_2 on Copper Surfaces”, The 7th International Symposium on Surface Science (ISSS-7), Shimane, Japan, November, 2014.

2. **Fahdzi Muttaqien**, Y. Hamamoto, K. Inagaki, and Y. Morikawa, “Dissociative Adsorption of CO_2 on Copper Surfaces”, The 1st International Symposium on Interactive Materials Science Cadet Program, Osaka, Japan, November, 2014.

3. **Fahdzi Muttaqien**, Y. Hamamoto, H. Kizaki, K. Inagaki, and Y. Morikawa, “Mechanistic Insight into CO_2 Dissociation on Copper Surface”, The 31st European Conference on Surface Science, Barcelona, Spain, August, 2015.

4. **Fahdzi Muttaqien**, S. Torii, Y. Hamamoto, H. Kizaki, K. Inagaki, and Y. Morikawa, "Formic Acid Decomposition on the Cu(111) Surface: van der Waals Density Functional Study", The 32nd European Conference on Surface Science, Grenoble, France, August, 2016.

5. **Fahdzi Muttaqien**, S. Makihara, Y. Hamamoto, K. Inagaki, and Y. Morikawa, "Dissociative adsorption of CO_2 on the Cu(111) and Cu(221) surfaces", The 69th Annual Meeting of Japan Physical Society (JPS), Kanagawa, Japan, March, 2014.

6. **Fahdzi Muttaqien**, Y. Hamamoto, H. Kizaki, K. Inagaki, and Y. Morikawa, "Complex Insight into CO_2 Dissociation on Copper Surfaces: Cu$-$O$-$Cu Chain and H_2O Effect", The 70th Annual Meeting of Japan Physical Society (JPS), Tokyo, Japan, March, 2015.

7. **Fahdzi Muttaqien**, Y. Hamamoto, H. Kizaki, K. Inagaki, and Y. Morikawa, "Role of Subsurface Hydrogen in Formate Hydrogenation on Flat and Stepped Cu Surfaces", The 71st Annual Meeting of Japan Physical Society (JPS), Tohoku, Japan, March, 2016.

8. **Fahdzi Muttaqien**, H. Oshima, Y. Hamamoto, K. Inagaki, I. Hamada, and Y. Morikawa, "Energy transfer dynamics of desorbed CO_2 in formate decomposition on Cu(111)", The 72nd Annual Meeting of Japan Physical Society (JPS), Osaka, Japan, March, 2017.